

## The mineral Dust Entrainment And Deposition (DEAD) model: Description and 1990s dust climatology

Charles S. Zender, Huisheng Bian, and David Newman

Department of Earth System Science, University of California at Irvine

**Abstract.** We describe a model for predicting the size-resolved distribution of atmospheric dust for climate and chemistry-related studies. The dust distribution from 1990–1999 is simulated with our mineral aerosol entrainment and deposition module embedded in a chemical transport model. Mobilization processes include entrainment thresholds for saltation, moisture inhibition, drag partitioning, and saltation feedback. For mobilization we assume soil texture is globally uniform and is replete with saltators. Soil erodibility is prescribed by a new physically based geomorphic index which is proportional to the runoff area upstream of each source region. Dry deposition processes include sedimentation and turbulent mix-out. Nucleation scavenging and size-resolved washout in both stratiform and convective cloud types are represented. Simulations of the 1990s broadly agree with station observations and satellite-inferred dust distributions. Without invoking anthropogenic mechanisms, the model captures the seasonal migration of the trans-Atlantic African dust plume, and the spring maximum in Asian dust outflow and concentration over the Pacific. We estimate the 1990s global annual mean and variability of  $D < 10 \mu\text{m}$  dust to be: Emissions,  $1490 \pm 160 \text{ Tg yr}^{-1}$ ; Burden,  $17 \pm 2 \text{ Tg}$ ; Optical depth at  $0.63 \mu\text{m}$ ,  $0.030 \pm 0.004$ . This emission, burden, and optical depth are significantly lower than some recent estimates. The model underestimates transport and deposition of East Asian and Australian dust to some regions of the Pacific Ocean. An underestimate of long range transport of particles larger than  $3 \mu\text{m}$  contributes to this bias. Our experiments support the hypothesis that dust emission “hot spots” exist in regions where alluvial sediments have accumulated and may be disturbed.

### 1. Introduction

<sup>1</sup>Mineral dust aerosol is involved in many important processes in Earth’s climate system. These processes include direct radiative forcing [Tegen *et al.*, 1996], nutrient transport [Martin, 1990; Swap *et al.*, 1992], land-use change [Nicholson *et al.*, 1998], and ecosystem health [Prospero, 1999; Shinn *et al.*, 2000]. Simulations of the distribution of mineral dust help improve our understanding of the role of dust in these processes, and the behavior of these processes in past, present, and future climates. In this paper we describe the

Dust Entrainment And Deposition (DEAD) model, designed for studying dust-related processes at both local and global scales. We present the underlying physical assumptions of DEAD and evaluate predictions of a 1990–1999 global natural dust simulation.

Models of the global distribution of mineral dust must successfully couple the microphysical processes of entrainment and deposition. In global models, soil and meteorological conditions are only available at coarse spatio-temporal resolution and with great uncertainties attached. Dust models are often differentiated by their representation of mobilization. At least two distinct classes of mobilization schemes exist. The simpler class parameterize mobi-

<sup>1</sup>Copyright 2003 by the American Geophysical Union.  
0148-0227/03/2002JD002775\$09.00

lization in terms of the third or fourth power of the wind speed or wind friction speed and then impose an empirical size distribution upon the emitted dust. We call these bulk mobilization schemes and they include *Tegen and Fung* [1994]; *Mahowald et al.* [1999]; *Perlwitz et al.* [2001]. The more complex class use complete microphysical specification of the erodible environment to predict the size-resolved saltation mass flux and resulting sandblasted dust emissions [*Marticorena and Bergametti*, 1995; *Shao et al.*, 1996; *Shao*, 2001]. Many of the input parameters for these fully microphysical schemes are not known globally, but these schemes have shown promising results in regional simulations *Shao and Leslie* [1997]; *Marticorena et al.* [1997]. Models intermediate in complexity between these two extremes, including the present model, are now in use at the global scale [*Ginoux et al.*, 2001; *Woodward*, 2001; *Luo et al.*, 2003]. Generally, these intermediate complexity dust models use microphysical parameterizations where possible, but make simplifying assumptions to produce adequate global simulations.

Herein we describe the physics and the mean climatology of the Dust Entrainment And Deposition (DEAD) model in the present climate. In this study, DEAD is implemented as a component of the Model for Atmospheric Chemistry and Transport (MATCH) Chemical Transport Model (CTM) [*Rasch et al.*, 1997], which is driven by National Center for Environment Prediction (NCEP) analyzed meteorology for the period 1990–1999 [*Kalnay*, 1996]. Using observational analyses (rather than predicted wind) minimizes meteorology-induced biases in the resulting dust distribution, and highlights deficiencies in the model representation of the mobilization and deposition processes. Quantifying these biases helps to reveal where more study is necessary.

Earlier versions of DEAD were used in aerosol assimilation studies of INDOEX [*Rasch et al.*, 2001; *Collins et al.*, 2001, 2002]. A modified version of DEAD has recently been used to study decadal variations in the 30-year dust record at Barbados [*Mahowald et al.*, 2002], the mean climatology of a 22-year time series [*Luo et al.*, 2003], and interannual variability in current climate dust production [*Mahowald et al.*, 2003]. Studies of the PRIDE and ACE-Asia field experiments are ongoing.

Section 2 describes the physical basis and formulation of the dust entrainment and deposition model. Section 3 presents the 1990–1999 simulated dust climatology and global budgets. Section 4 evaluates the simulated dust climatology with station observations of dust concentration, deposition, and optical depth. Section 5 summarizes our results and their implications for future research.

## 2. Dust Prediction

Predicting the distribution of mineral dust in the atmosphere requires representation of source, sink, and transport processes. The source process for dust is mobilization by wind. Sink processes are dry deposition (gravitational sedimentation and turbulent mix-out), and wet deposition (in-cloud and below cloud scavenging). These processes are described in this section.

Dust is advected and diffused as a passive scalar quantity by the transport processes and methods used in the host model. For MATCH, these processes include mixing within the planetary boundary layer [*Holtstag and Boville*, 1993], shallow convective transport [*Hack*, 1994], a plume ensemble method of deep convection [*Zhang and McFarlane*, 1995], and advection by large scale winds [*Rasch et al.*, 2001]. These transport mechanisms are nearly identical in both the MATCH and the Community Climate Model (CCM) versions of DEAD.

### 2.1. Mobilization

Adequate representation of the long-lived dust burden requires careful attention to the process of dust mobilization [*Schulz et al.*, 1998]. A large number of factors, many of them poorly known on a global scale, determine soil erodibility and dust emissions. The most important factors include wind friction speed, vegetation cover, and surface soil moisture content. We generally follow the microphysical and micrometeorological approach to dust mobilization developed by *Marticorena and Bergametti* [1995], hereafter MaB95.

Dust entrained into the atmosphere originates in source soils which contain the clay-sized ( $D_p < 2.5 \mu\text{m}$ ) and silt-sized ( $2.5 < D_p < 60 \mu\text{m}$ ) particles whose atmospheric residence time exceeds about 20 min (i.e., the temporal resolution of the host model). However, clay and silt-sized particles are not directly mobilized by the wind because cohesive forces (e.g., capillary and electrostatic) bind these particles tightly to the soil. Laboratory [*Iversen and White*, 1982] and field [*Shao et al.*, 1996] wind tunnel studies show that dust is primarily injected into the atmosphere during the sandblasting caused by saltation bombardment [*Alfaro and Gomes*, 2001; *Grini et al.*, 2002]. Sandblasting refers to the disaggregation and ejection of clay and silt particles by saltating sand-sized particles ( $D_p > 60 \mu\text{m}$ ).

The first steps of the source scheme are therefore the prediction of saltation events and their intensity. The condition for saltation initiation is that the turbulent drag of the surface atmosphere dissipates enough momentum to overcome the gravitational inertia of sand-sized particles. The solution of the boundary layer turbulence problem provides required

surface drag properties in the form of the modeled wind friction speed  $u_*$ . To obtain a  $u_*$  suitable for dust mobilization, DEAD re-solves the boundary layer turbulence problem independently of the host model (i.e., MATCH) using boundary conditions more suitable for dust producing regions. The surface roughness length in dust producing regions is set to the globally uniform value of  $z_{0,m} = 100 \mu\text{m}$ , a value more typical of erodible soil beds [Gillette *et al.*, 1997] than the large scale roughness lengths for bare ground ( $z_{0,m} \sim 5 \text{cm}$ ) used in general circulation models [e.g., Bonan, 1996]. We obtain the kinematic and thermodynamic properties of the boundary layer by assuming that the surface and atmosphere constantly adjust surface heat, vapor, and momentum exchanges in order to maintain thermal equilibrium with the radiation field [Bonan, 1996].

## 2.2. Threshold Friction Velocity

The mass flux of saltating particles  $Q_s$  (see Equation (10), below) depends on the excess of the wind friction speed  $u_*$  over the threshold wind friction speed for saltation,  $u_{*t}$ . The relation between soil particle size and  $u_{*t}$  has been measured in wind tunnels [Bagnold, 1941; Greeley and Iversen, 1985; Shao *et al.*, 1996; Batt and Peabody II, 1999]. Iversen and White [1982] developed a semi-empirical parameterization of this relationship in terms of the threshold friction Reynolds number  $\text{Re}_{*t} \equiv u_{*t}D/\nu$  where  $\nu$  is the kinematic viscosity of air. DEAD employs this parameterization in the computationally amenable form

$$u_{*t}(D) = \left\{ \begin{array}{l} \left[ \frac{0.1666681\rho_p g D}{-1+1.928\text{Re}_{*t}^{0.0922}} \left( 1 + \frac{6 \times 10^{-7}}{\rho_p g D^{2.5}} \right) \right]^{1/2} \rho^{-1/2} \\ \left[ 0.0144\rho_p g D (1 - 0.0858e^{-0.0617(\text{Re}_{*t}-10)})^2 \right]^{1/2} \end{array} \right. \quad (1)$$

Expression (1) is arranged so that all the microphysical properties are in the first term on the right hand side. This term contains all properties determined by soil size and density and thus needs to be evaluated only once (at model start) for a given saltating particle size. The  $\rho^{-1/2}$  term is the same for all particle sizes, but depends on ambient, time-varying environmental conditions. Since  $\text{Re}_{*t}$  is defined in terms of  $u_{*t}$ , (1) is an implicit definition of  $u_{*t}$  which must be solved iteratively.

The optimal particle size for saltation  $D_0$  occurs where  $u_{*t}$  is at a minimum. Solutions to (1) show that, for typical conditions on Earth,  $D_0 \approx 75 \mu\text{m}$  [Iversen and White, 1982]. Following MaB95, we assume all soils in erodible regions contain particles of size  $D_0$ , so that saltation is initiated whenever  $u_* > u_{*t}(D_0)$ . To accelerate solution of (1), we compute  $u_{*t}(D_0)$  using the non-iterative parameterization for  $\text{Re}_{*t}$  introduced in MaB95.

Three processes modify  $u_*$  and  $u_{*t}$ : drag partitioning,

the Owen effect, and moisture inhibition. First, a drag partition parameterization is applied to represent the sink of atmospheric momentum into non-erodible roughness elements [Raupach, 1992]. We consider two roughness lengths pertinent to dust emissions from erodible surfaces. The first is the aerodynamic roughness length of the bare ground including the non-erodible elements such as pebbles, rocks, and vegetation. This is traditionally known as the roughness length for momentum transfer,  $z_{0,m}$ . The second roughness length is the so-called “smooth” roughness length,  $z_{0,m}^s$  [Marticorena and Bergametti, 1995].  $z_{0,m}^s$  is the roughness length of a bed of potentially erodible particles without any non-erodible elements. Wind tunnel experiments over uniform beds comprised of known particle sizes show that

$$z_{0,m}^s \approx D/30 \quad (2)$$

We use globally uniform values for  $z_{0,m}$  and  $z_{0,m}^s$  of  $100.0 \mu\text{m}$  and  $33.3 \mu\text{m}$ , respectively. From (2), this corresponds to particle beds of particle area-mean size of  $D \sim 1 \text{mm}$ .

The efficiency with which drag is partitioned between erodible and non-erodible soils is expressed as an increase  $f_d$  in the threshold friction speed for saltation  $u_{*t}$  [Marticorena and Bergametti, 1995]

$$f_d = \left[ 1.0 - \left( \frac{\ln(z_{0,m}/z_{0,m}^s)}{\ln\{0.35[(0.1/z_{0,m}^s)^{0.8}]\}} \right) \right]^{-1} \quad (3)$$

The second process which modifies  $u_*$  and  $u_{*t}$  is the Owen effect—the positive feedback of saltation upon surface roughness length and friction speeds [Owen, 1964]. Based on field measurements at Owens Dry Lake, California, Gillette *et al.* [1998] found that the increase in wind friction speed due to saltation varies quadratically with the difference between the 10 m wind speed  $U_{10}$  and the threshold wind speed at 10 m  $U_{10,t}$  as

$$u_{*,s} = u_* + 0.003(U_{10} - U_{10,t})^2 \quad (4)$$

The Owen effect,  $\Delta u_* = u_{*,s} - u_*$ , affects only the saltation fluxes and does not affect heat, moisture, and momentum exchange in the large scale host model. This approximation will be removed in future versions of DEAD.

Finally, the inhibition of saltation by soil moisture is accounted for by increasing  $u_{*t}$  in moist soils. A number of investigators have created simple parameterizations which account for the increase of  $u_{*t}$  with soil water [Belly, 1964; Pye, 1987; Gillette, 1988; Selah and Fryrear, 1995; Shao *et al.*, 1996; Fécan *et al.*, 1999]. We adopt the parameterization of Fécan *et al.* [1999] who used measurements to specify free parameters in the adsorptive theory of McKenna-Neuman and Nickling [1989]. In our model, the capillary

force suppresses dust deflation when the near-surface soil gravimetric water content  $w$  exceeds a threshold  $w_t$  determined by

$$w_t = a(0.17M_{\text{clay}} + 0.14M_{\text{clay}}^2) \quad (5)$$

where the parenthetical factor is directly from *Fécan et al.* [1999] and  $a$  is an ad hoc factor chosen to improve model simulations. The increase  $f_w$  in threshold friction velocity for saltation  $u_{*t}$  due to soil water is [*Fécan et al.*, 1999]

$$f_w = \begin{cases} 1 & : w \leq w_t \\ \sqrt{1 + 1.21[100(w - w_t)]^{0.68}} & : w > w_t \end{cases} \quad (6)$$

In these simulations, the CTM uses upper layer volumetric soil water content  $\theta \text{ m}^3 \text{ m}^{-3}$  interpolated from the 6-hourly NCEP/NCAR reanalysis data. It is necessary to convert the NCEP volumetric water content  $\theta$  to the gravimetric water content (dry mass basis)  $w \text{ kg kg}^{-1}$  used in (5) and (6). This requires knowledge of the volume of air (pores) per unit volume soil. We assume that the volumetric water content of the soil at saturation,  $\theta_s \text{ m}^3 \text{ m}^{-3}$  equals the porous volume of air in dry soil, i.e., soil is saturated when all interparticle pores are filled with water. Under this assumption, the equivalence between  $\theta$  and  $w$  is

$$\theta_s = 0.489 - 0.126M_{\text{sand}} \quad (7)$$

$$\rho_{b,d} = \rho_p(1.0 - \theta_s) \quad (8)$$

$$w = \theta\rho_l/\rho_{b,d} \quad (9)$$

where  $M_{\text{sand}} \text{ kg kg}^{-1}$  is the mass fraction of sand in the soil [*Bonan, 1996; Global Soil Data Task, 1999*],  $\rho_p = 2500 \text{ kg m}^{-3}$  is the mean soil particle density,  $\rho_l = 1000 \text{ kg m}^{-3}$  is the density of liquid water, and  $\rho_{b,d} \text{ kg m}^{-3}$  is the bulk density of dry soil. Thus sandier soils have smaller  $w$  for a given  $\theta$ .

The NCEP soil moisture  $w$  usually exceeds  $0.1 \text{ m}^3 \text{ m}^{-3}$  over active dust emission regions all year long. We have found empirically that setting  $a = 5$  in (5) gives reasonable results in global scale models driven by NCEP  $w$ . The NCEP  $\theta$  is only available at two model layers, every six hours, and is based on a soil texture, hydrologic model, and precipitation fields that differ from those employed in DEAD and MATCH, respectively. This inconsistency is a potential cause of bias in our results. Embedding DEAD in a host model with a consistent land surface representation removes this inconsistency.

### 2.3. Saltation and Dust Production

Primary dust production, i.e., the direct mobilization of small particles by wind, is negligible on Earth because  $u_{*t}(D)$  (1) is usually too large [*Greeley and Iversen, 1985*].

Instead, the vertical flux of fine dust is dominated by a secondary process called sandblasting, which refers to the release of small particles by large particles in saltation [*Gomes et al., 1990*]. Sandblasting and disaggregation of small clay and silt-sized particles from the surface and from larger particles during saltation is strongly sensitive to the size distribution of saltating particles [*Shao et al., 1996; Grini et al., 2002*].

DEAD simulates the total horizontally saltating mass flux of large particles  $Q_s$  according to the theory of *White* [1979]

$$Q_s = \frac{c_s \rho u_*^3}{g} \left(1 - \frac{u_{*t}}{u_*}\right) \left(1 + \frac{u_{*t}}{u_*}\right)^2 \quad (10)$$

where,  $c_s = 2.61$ ,  $\rho$  is the atmospheric density,  $u_*$  is the wind friction speed,  $g$  is acceleration of gravity, and  $u_{*t}$  is the threshold wind friction speed. This relationship assumes linearity between the vertical mass flux of saltators and the wind friction excess  $u_* - u_{*t}$ , an assumption borne out by microphysical saltation models as well as wind tunnel studies [*White, 1979*]. DEAD assumes that total  $Q_s$  (10) is determined solely by the threshold friction speed for the optimal particle size  $u_{*t}(D_0)$  (1). More detailed models predict a size-resolved  $Q_s$  [*Shao and Leslie, 1997; Marticorena et al., 1997*], but this requires global knowledge of the parent soil texture.

The horizontal (saltation) mass flux  $Q_s$  (10) is converted to a vertical dust mass flux  $F_d$  with an efficiency  $\alpha$ , called the sandblasting mass efficiency [*Alfaro et al., 1997*], i.e.,  $F_d = \alpha Q_s$ . Observations reveal that  $F_d$  exhibits high sensitivity to parent soil texture [*Shao et al., 1993*] and wide scatter with increasing  $u_*$  [*Alfaro and Gomes, 2001; Grini et al., 2002*]. DEAD adopts the size- and drag-independent  $\alpha$  parameterization of MaB95

$$\alpha = 100 \exp[(13.4M_{\text{clay}} - 6.0) \ln 10] \quad (11)$$

where the mass fraction of clay particles in the parent soil is restricted to  $M_{\text{clay}} < 0.20$ . The sandblasting mass efficiency  $\alpha$  (11) increases by nearly three orders of magnitude as the parent soil texture changes from  $M_{\text{clay}} = 0.0$  (sand) to 0.20 (sandy loam). This parameterization yields reasonable results when applied in regional models [*Marticorena et al., 1997*] where soil characterization is reliable, but proves overly sensitive to  $M_{\text{clay}}$  in our global model. Therefore we use a globally uniform value of  $M_{\text{clay}} = 0.2$  to determine  $\alpha$  in (11). Without this assumption, dust emissions, burden, and optical depth would be 2–15 times higher in East Asia relative to North Africa, significantly degrading the fidelity of the simulation. This assumption will be relaxed when more reliable global erodible soil datasets become available.

Currently we use the IGBP soil texture dataset [*Global Soil Data Task*, 1999]. This dataset has less clay in the Saharan region of Africa than the soil dataset of *Webb et al.* [1993]. The sandier IGBP soils have a reduced threshold for evapotranspiration, and consequently allow drier surfaces.

DEAD assumes that saltation leads to dust production whenever  $u_* > u_{*t}(D_0)$  over bare ground. This assumption means that soils depleted in particles of size  $D_0$  will begin saltation at unrealistically low wind friction speeds.

The physics of entrainment in global dust models differ significantly. It is helpful to summarize the basic differences so that the origin of inter-model differences may be understood. Many earlier studies *Genthon* [1992]; *Tegen and Fung* [1994]; *Mahowald et al.* [1999] based  $F_d(D)$  on a cubic or quartic relationship with wind speed  $U$ . A uniform threshold wind speed  $U_t$  was commonly used. *Woodward* [2001] predicts a saltation flux  $Q_s(D)$  (10) for each dust size class by assuming the saltation layer mass distribution equals the parent soil mass distribution. These horizontal fluxes  $Q_s(D)$  are converted to vertical fluxes using the local soil clay content as in (11). *Ginoux et al.* [2001] do not explicitly model saltation. Instead, they apply a size-dependent threshold velocity  $u_{*t}$  for dust particles (rather than saltation-sized particles) which decreases with decreasing particle size. In effect, the wind directly entrains dust-sized particles into the atmosphere. This allows small dust particles to be entrained by weak wind events, relative to wind tunnel observations [*Iversen and White*, 1982].

#### 2.4. Particle Size Distributions

DEAD uses a bin-method to independently transport discrete, non-interacting, size (mass) classes. Each bin has an independently configurable sub-bin distribution which allows more accurate treatment of particle number and optical properties when the number of transport bins is small. The number of transport bins is arbitrary, limited only by the computational requirements of the model. Although the entrainment of mineral dust aerosol is initiated by the saltation of sand-sized particles, only particles with sizes  $D_p \lesssim 10 \mu\text{m}$  reside in the atmosphere long enough to travel significant distances downwind. The vertical dust flux  $F_d$  obtained from (10) and (11) is assumed to be size-distributed in an analytic, tri-modal lognormal probability density function (PDF) which is globally uniform. This PDF comprises the ‘‘Background’’ modes of dust suggested by *D’Almeida* [1987]. These three modes are hereafter called the source modes. Table 1 lists the parameters of dust in the source regions. Shown are the number median diameter  $\tilde{D}_n$ , mass median diameter  $\tilde{D}_v$ , geometric standard deviation  $\sigma_g$ , and mass fraction  $M$  of each mode. Note that the middle mode, which dominates long range transport, has  $\sigma_g = 1.9$ , which

**Table 1. Tri-modal Size Distribution in Source Regions<sup>a</sup>**

$\tilde{D}_n$ $\mu\text{m}$	$\tilde{D}_v$ $\mu\text{m}$	$\sigma_g$ fraction	$M$ fraction
0.16	0.832	2.10	0.036
3.19	4.82	1.9	0.957
10.0	19.38	1.6	0.007

<sup>a</sup>Background dust mode of *D’Almeida* [1987]

is close to the  $\sigma_g = 2.0$  found to produce good agreement in visible optical depth with satellite observations [*Schulz et al.*, 1998].

The host model carries dust in  $J$  transport bins. The number  $J$  is empirically chosen to balance computational resources against desired accuracy in the prediction of dust particle number, surface area, and volume (mass). As a bin method, this procedure converges to an exact representation of transport of the source modes as  $J$  increases. The mass fraction of each source mode  $i$  that is carried in each sink (transport) bin  $j$  is the mass overlap  $M_{i,j}$ . Since the mass in the source modes is assumed to be lognormally distributed, the  $M_{i,j}$  are [*Schulz et al.*, 1998]

$$M_{i,j} = \frac{1}{2} \left[ \text{erf} \left( \frac{\ln(D_{\max,j}/\tilde{D}_{v,i})}{\sqrt{2} \ln \sigma_{g,i}} \right) - \text{erf} \left( \frac{\ln(D_{\min,j}/\tilde{D}_{v,i})}{\sqrt{2} \ln \sigma_{g,i}} \right) \right] \quad (12)$$

where erf is the standard error function,  $D_{\min,j}$  and  $D_{\max,j}$  are the minimum and maximum diameters of bin  $j$ , and  $\tilde{D}_{v,i}$  and  $\sigma_{g,i}$  are the mass median diameter and geometric standard deviation of the source modes (Table 1). The total transported mass fraction of the source modes is  $\sum \sum M_{i,j} = M$ . If all of the mass in the  $I$  source modes is contained in the size range  $[D_{\min,0}, D_{\max,J}]$  then  $M = 1$ . In the present study,  $0.1 < D < 10.0 \mu\text{m}$  and  $M = 0.87$ . The residual, non-transported mass (i.e., 13%) is almost all in the coarse mode centered at  $19 \mu\text{m}$  (Table 1) which is not important for long range transport [*Schulz et al.*, 1998].

Within each transport bin, particles are assumed to have an analytic, time-invariant, sub-bin distribution. While the absolute mass in each bin changes every timestep due to size dependent source and sink processes (e.g., sedimentation), the assumed sub-bin distribution within each bin never changes. Figure 1 shows the simulated transported size distribution at Barbados for July. Approximately 80% of the transported mass is in sizes  $D > 2.5 \mu\text{m}$  in African source regions. Sedimentation and preferential scavenging of large

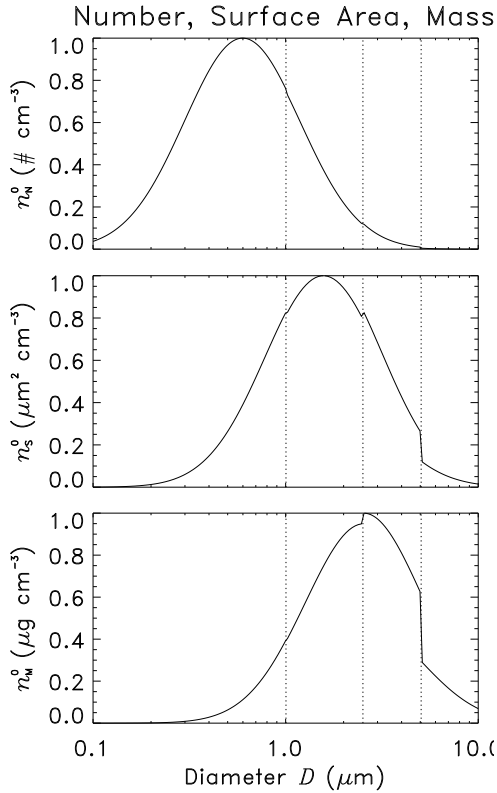


**Figure 1.** Predicted normalized size distribution at Barbados in July. Transport bins are separated by dashed vertical lines. Solid curve shows prescribed sub-bin number, surface area, and mass distribution.

particles (see Table 3 below) has reduced the mass in the silt bins relative to the clay bins during transport, but the assumed sub-bin distributions of number, surface area, and mass have not changed. Only 50% of the mass remains in silt sizes at the surface in Barbados. As discussed in § 5, the transport mode of African dust has recently been estimated as about  $\bar{D}_v = 3.5 \mu\text{m}$  or larger [Reid et al., 2003].

We employ the long range transport mode observed by Shettle [1984] ( $\bar{D}_v = 2.524 \mu\text{m}$ ), as modified by Schulz et al. [1998] ( $\sigma_g = 2.0$ ), for the sub-bin distribution of all transport bins. Thus the modeled dust transport is the most realistic for the long range transport mode, exactly where it is most important. Table 2 lists the size grid, sub-bin distribution parameters, and bin-mean physical properties for the  $J = 4$  transport bins used in the model. Shown are minimum size  $D_{\min}$ , maximum size  $D_{\max}$ , volume median  $\bar{D}_v$  and geometric standard deviation  $\sigma_g$  of sub-bin distribution, specific (i.e., per unit mass) number  $\bar{N}$ , surface area  $\bar{S}$ , scattering  $\psi_s$ , extinction  $\psi_e$ , and mass fraction of entrained and transported dust  $M_j$ , in each bin. For large  $J$

the sub-bin distribution is not important, since physical parameters do not vary greatly across the bin width. Sub-bin distribution is important when  $J$  is chosen to be small for computational efficiency ( $J = 4$  in the present study). The analytic sub-bin distribution allows accurate prescription of physical properties known to vary significantly across the bin width. For example, the visible mass extinction coefficient  $\psi_e$  varies between  $125\text{--}3600 \text{ m}^2 \text{ kg}^{-1}$  for dust particle sizes  $0.1 < D_p < 1.0 \mu\text{m}$ . The value used for the entire bin is  $\psi_e = 2893 \text{ m}^2 \text{ kg}^{-1}$ , corresponding to extinction by monodisperse particles of size  $D = 0.37$  or  $0.84 \mu\text{m}$ .

All time-independent size-varying properties (extinction, scavenging cross-sections, sedimentation velocities) are computed on a high resolution size grid, then weighted by the appropriate sub-bin distribution (surface area for extinction, volume for sedimentation), and then integrated to bin-mean values. The bin-mean value shown in Table 2 is used in all successive timesteps. The bin boundaries at  $2.5$  and  $10.0 \mu\text{m}$  facilitate comparison with U.S. PM2.5 and PM10 standards.

## 2.5. Optical Properties

Optical properties of mineral dust are required to compare modeled dust distributions with remote sensing data, and to predict radiative feedbacks from dust in coupled models. There is great uncertainty in mineral dust optical properties for many reasons [Sokolik et al., 2001]. For instance, long range transported mineral dust is generally not a pure crystal (e.g., quartz), but rather an internal mixture of many minerals [e.g., Pye, 1987] which is regionally dependent. Moreover, transported dust undergoes chemical processing by gases and other species leading to coated, multi-component aerosols in the long range mode [Dentener et al., 1996]. As a result, treating dust measured in different regions with different techniques leads to large uncertainties in radiative forcing [Sokolik and Toon, 1996]. Fortunately, the total extinction coefficient of dust is much less uncertain than the individual scattering and absorbing components of dust, especially at visible wavelengths. In this study we use the visible indices of refraction for dust measured by Patterson [1981],  $n = n_r + in_i = 1.56 + 0.0038i$  at  $0.63 \mu\text{m}$ . This is very close to  $n = 1.56 + 0.0033i$  at  $0.625 \mu\text{m}$  measured in Afghanistan [Sokolik et al., 1993]. It is, however, generally more refractive and absorptive than annual mean values at  $0.67 \mu\text{m}$  inferred from AERONET measurements [Holben et al., 1998] at dusty stations (Bahrain, Saudi Arabia, Cape Verde, Banzoumbou, Ougadougou, Barbados, and Mongolia) where  $1.43 < n_r < 1.56$  and  $0.001 < n_i < 0.0027$  (O. Dubovik, personal communication, 2001). The AERONET values appear to be influenced by aged dust with a significant water or organic component, and do not necessarily represent dry dust itself, the focus of this study. The specific scattering and

**Table 2. Transport Bins and Sub-Bin distribution Parameters<sup>a</sup>**

Bin	$D_{\min}$ $\mu\text{m}$	$D_{\max}$ $\mu\text{m}$	$\tilde{D}_V$ $\mu\text{m}$	$\sigma_g$	$\frac{N}{\text{kg}^{-1}}$	$\frac{S}{\text{m}^2 \text{kg}^{-1}}$	$\psi_s$ $\text{m}^2 \text{kg}^{-1}$	$\psi_e$ $\text{m}^2 \text{kg}^{-1}$	$M_j$ %
1	0.1	1.0	2.524	2.0	$3.484 + 15$	$3.464 + 03$	$2.834 + 03$	$2.893 + 03$	3.2
2	1.0	2.5	2.524	2.0	$2.138 + 14$	$1.471 + 03$	$7.779 + 02$	$8.350 + 02$	17
3	2.5	5.0	2.524	2.0	$2.205 + 13$	$7.107 + 02$	$3.343 + 02$	$3.825 + 02$	41
4	5.0	10.0	2.524	2.0	$3.165 + 12$	$3.741 + 02$	$1.705 + 02$	$1.961 + 02$	38

<sup>a</sup>Interpret  $3.484 + 15$  as  $3.484 \times 10^{15}$ .

extinction coefficients that result for each size bin of dust are shown in Table 2.

The adequacy of these optical properties for the present purposes is confirmed by comparison to in situ estimates of the scattering properties of long range transported African dust. *Li et al.* [1996] measured the specific scattering efficiency of ashed Saharan dust at Barbados to be  $\psi_s = 770 \text{ m}^2 \text{ kg}^{-1}$  at 530 nm. Since dust is about 130% of ash by weight, this is equivalent to  $\psi_s \sim 590 \text{ m}^2 \text{ kg}^{-1}$  for dust. *Maring et al.* [2000] estimate  $\psi_s = 610 \pm 100 \text{ m}^2 \text{ kg}^{-1}$  at 550 nm for dust in Barbados. For comparison, the July mean dust distribution shown in Figure 1 has  $\psi_s = 720 \text{ m}^2 \text{ kg}^{-1}$  at 550 nm. The modeled scattering efficiency of long range Saharan dust is thus about 20% too high, but close to the measurement uncertainty. The inefficient long range transport of large dust particles, previously mentioned, contributes to this bias since the visible specific scattering efficiency decreases with increasing particle size for  $D > 1 \mu\text{m}$ .

## 2.6. Land Surface and Geographic Constraints

Many significant dust plumes emanate from completely barren regions, e.g., the Sahara desert or Saudi Arabian peninsula. There are, however, significant sources of dust in semi-arid regions where vegetation may act as a primary dust constraint, e.g., the Sahel [*Teegen and Fung, 1995; Mbourou et al., 1997*]. Moreover, significant amounts of bare ground exist in temperate regions where dust emissions are minimal. It is therefore important to account for emission constraints by vegetation and by snow. The fraction of bare soil exposed in a gridcell  $A_m$  and thus suitable for mobilization is the maximally overlapped product of the fractions of dry ground, non-snow-covered ground, and non-vegetated ground

$$A_m = (1 - A_l - A_w)(1 - A_s)(1 - A_v) \quad (13)$$

where  $A_l$  and  $A_w$  are the fractions of land covered by lakes and wetlands, respectively [*Cogley, 1991; Bonan, 1996*],  $A_s$

is the snow-covered fraction of ground, and  $A_v$  is the fraction of ground covered by vegetation.

Vegetation acts to constrain mineral dust emissions in multiple ways, which is why vegetation is a primary strategy to reduce soil erosion [e.g., *Nicholson et al., 1998*]. First, standing vegetation and litter compete with bare ground as sinks for atmospheric momentum. This drag partitioning results in less drag on the erodible component of the surface [*Raupach, 1994*], because the canopy acts as a windbreak for the surface. Second, plant shade and root systems are effective at trapping soil moisture [e.g., *Hillel, 1982*]. This plant-induced soil moisture constraint is implicitly accounted for by (6). We assume that vegetation acts to constrain dust by linearly reducing the fraction of bare soil  $A$  exposed in a gridcell.

$$A_v = \min[1.0, \min(V, V_t)/V_t] \quad (14)$$

where  $V$  is the vegetation area index, the sum of the (one-sided) leaf plus stem area index. Thus  $A_v = 0$  for  $V = 0 \text{ m}^2 \text{ m}^{-2}$  and  $A_v = 1$  for  $V \geq V_t$ . The threshold for complete suppression of dust emissions is set to  $V_t = 0.3 \text{ m}^2 \text{ m}^{-2}$ , a reasonable value based on previous studies [*Mahowald et al., 1999*]. We use a global vegetation dataset which supplies monthly leaf area index derived from 1 km satellite data [*Kergoat et al., 1999; Bonan et al., 2002*].

A similar constraint is imposed for the horizontal fraction of ground covered by snow,  $A_s$ , and thus unavailable for dust entrainment. Snow coverage is derived from the liquid water equivalent snow depth  $h_l$  provided by the analyses (or model). We assume the bulk density of snow is  $\rho_s = 100 \text{ kg m}^{-3}$ , a reasonable value for fresh, non-packed snow [*Wiscombe and Warren, 1980*] which is most relevant to dust emissions constraints.

$$h = h_l \rho_l / \rho_s \quad (15)$$

$$A_s = \min(h/h_t, 1.0) \quad (16)$$

where  $h$  is the geometric snow thickness and  $h_t = 0.05 \text{ m}$

is the thickness for 100% snow coverage [Bonan, 1996] and dust suppression (13).

Satellite-based retrievals of proxies for absorbing aerosol over land have revolutionized our understanding of mineral dust emission constraints. As suggested by J. M. Prospero, the TOMS absorbing aerosol index [Herman et al., 1997] provides strong evidence that climatologically strong dust emission regions, so-called “hot spots”, coincide with topographic depressions where alluvial sediments have accumulated [Gillette, 1999; Prospero et al., 2002]. Ginoux et al. [2001] parameterized this hypothesis in terms of a source erodibility factor  $S$ , defined as the fifth power of the ratio of the local height above a regional minimum height to the total elevation range of the surrounding  $10^\circ \times 10^\circ$  region. This definition of  $S$  does not replicate the hydrological definition of an alluvial basin because it is based on a discontinuous function of elevation rather than on hydrological channels for surface runoff.

Our time-independent erodibility factor is also based on the alluvial sediment/disturbance hypothesis, but represents the hydrologic processes involved more realistically. We quantify  $S$  as the upstream area from which sediment transported in surface runoff may have accumulated. We computed this upstream area from a Digital Elevation Map (NGDC TerrainBase 5 minute resolution) using the two step procedure described in Jenson and Domingue [1988]. Since estimates of surface runoff are explicitly not included in  $S$ , we call this  $S$  a geomorphic, rather than topographic or hydrologic, erodibility factor. A complete description and inter-comparison of the geomorphic and other erodibility factors is presented in Zender et al. [2003]. Use of a spatially heterogeneous  $S$ , whether ours or that of Ginoux et al. [2001], dramatically improves the spatial correlation of simulated emissions with TOMS satellite indices of absorbing aerosols relative to simulations with no erodibility factor [Zender et al., 2003].

Without correction DEAD predicts some small, geographically disparate sources where all the criteria are met (17) but where satellite data do not show climatologically strong dust burdens [Prospero et al., 2002] and surface data are lacking. These questionable “hot spots” are concentrated along or near the coasts of Greenland, Hudson’s Bay, Northern Siberia, and Northern Europe and are highly dependent on the land cover (vegetation) dataset employed. These polar sources would not contribute much to dust loading, as they are generally washed out very quickly, but they can contribute up to 5–10% of surface fluxes. Rather than allowing these dubious sources to influence our global simulations, we removed them by zeroing the erodibility factor  $S$  along coasts and north of  $60^\circ\text{N}$ . Ruling out apparently spurious sources in a model using *ad hoc* criteria (e.g., lo-

cation or mean relative humidity), does conceal weaknesses in the model physics and/or boundary datasets. These questionable sources may be actual dust sources that do not show up in TOMS imagery due to weak strength, low absorption index, or thick boundary layers [Herman et al., 1997; Torres et al., 1998; Mahowald and Dufresne, 2004]. They may also be dormant or potential sources which are close to activation or are anthropogenically constrained in the present climate.

## 2.7. Dust Entrainment

Summarizing the physical processes described in the preceding sections, the total vertical mass flux of dust  $F_{d,j}$  into transport bin  $j$  is

$$F_{d,j} = TA_m S \alpha Q_s \sum_{i=1}^I M_{i,j} \quad (17)$$

where the summation is over the  $I = 3$  source modes. A global tuning factor,  $T$ , is chosen to give a reasonable climatological simulation. The global mean  $F_{d,j}$  depends on the horizontal and temporal resolution of the model primarily due to the non-linearity of  $Q_s$  with wind speed. These simulations set  $T = 7.0 \times 10^{-4}$ , resulting in a global annual entrainment of about  $1500 \text{ Tg yr}^{-1}$  of fine dust ( $D < 10 \mu\text{m}$ ) into the atmosphere.

## 2.8. Dry Deposition

The simulation of dry deposition of mineral aerosol particles requires accurate specification of the gravitational settling and turbulent mix-out of particles ranging from  $0.1 < D_p < 10.0 \mu\text{m}$ .

**2.8.1. Gravitational Settling** Particles are assumed to settle gravitationally at their terminal velocity  $v_g$  and to reach this velocity instantaneously.

$$v_g = \left( \frac{4gDC_c\rho_p}{3C_D\rho} \right)^{1/2} \quad (18)$$

where the slip correction factor  $C_c$  and the drag coefficient  $C_D$  are given by Seinfeld and Pandis [1997]. In general  $C_D$  is a function of  $v_g$  so (18) is an implicit equation for  $v_g$ . An iterative solution to (18) is straightforward but too time consuming for large scale atmospheric models. The following Stokes approximation provides a solution.

For Reynolds numbers  $\text{Re} < 0.1$  particles obey the Stokes settling velocity  $u_{\text{St}}$

$$u_{\text{St}} = \frac{D^2\rho_p g C_c}{18\mu} \quad (19)$$

where  $\mu$  is the dynamic viscosity of air. The present study is limited to the size range  $0.1$  to  $10.0 \mu\text{m}$ , where the Stokes

velocity  $u_{St}$  is an excellent approximation to the terminal velocity  $v_g$ . However, the Stokes velocity overestimates sedimentation by more than 10% for  $D > 20 \mu\text{m}$ . The model is capable of simulating saltation and dust production of particle sizes up to about  $1000 \mu\text{m}$ . For large particle sizes, we define a time-invariant Stokes correction factor  $C_{St}$  as

$$C_{St} = v_g/u_{St} \quad (20)$$

The  $C_{St}$  correction exceeds 10% for mineral particles larger than  $45 \mu\text{m}$ . At startup, the model computes  $C_{St}(D, p_0, T_0)$  (20) for each size at a temperature and pressure representative of arid erosion regions on Earth (currently  $p_0 = 1000 \text{ mb}$  and  $T_0 = 295 \text{ K}$ ). The model computes  $u_{St}$  (19) every timestep and applies the time-invariant correction factor  $C_{St}(D, p_0, T_0)$  to obtain  $v_g$ . In this manner the iterative solution to (18) at every timestep is avoided.

**2.8.2. Turbulent mix-out** Turbulent deposition is treated using the resistance-in-series method [e.g., *Wesely, 1989*]. The turbulent deposition velocity  $v_t$

$$v_t = \frac{1}{r_a + r_b + r_a r_b v_g} \quad (21)$$

where the aerodynamic resistance through the constant flux layer  $r_a$  accounts for local stability effects using similarity theory as in *Bonan [1996]*. While  $r_a$  is independent of particle size, the quasi-laminar layer resistance  $r_b$  depends on a particle's microphysical characteristics

$$r_b = \frac{1}{u_* (Sc^{-2/3} + 10^{-3}/St)} \quad (22)$$

The Schmidt number  $Sc$  in the denominator accounts for Brownian diffusion and is dominant for  $D \lesssim 0.7 \mu\text{m}$ . The Stokes number  $St$  accounts for inertial impaction and becomes important for  $D \gtrsim 5 \mu\text{m}$ . The resistance to particle or gaseous diffusion across the quasi-laminar layer to a solid surface is proportional to  $Sc^{-2/3}$  [*Slinn et al., 1978*]. The rate-limiting resistance for turbulent mix-out of accumulation mode particles is  $r_b$  for all wind speeds. For coarser particles ( $D \gtrsim 2 \mu\text{m}$ ),  $r_b$  is the limiting resistance for weak wind speeds, but  $r_a$  becomes the limiting resistance as  $U$  increases above about  $5 \text{ m s}^{-1}$ .

## 2.9. Wet Deposition

Wet deposition or scavenging of particles by water is the dominant deposition process for small dust particles because dry deposition processes are very inefficient for  $D < 2 \mu\text{m}$ , i.e., the accumulation mode [e.g., *Seinfeld and Pandis, 1997*]. The model distinctly treats four types of wet deposition: Particles in precipitating clouds may be removed

by nucleation scavenging, which accounts for particles becoming embedded in raindrops. Particles beneath precipitating clouds are susceptible to sub-cloud scavenging (collision scavenging), which accounts for collection of particles by precipitation. Nucleation and sub-cloud scavenging are each treated separately for convective and for stratiform precipitation.

Evaporation of stratiform precipitation releases scavenged dust in direct proportion to the mixing ratio of dust in the precipitation and the local rain evaporation rate. The evaporation tendency is consistent with the hydrologic cycle of the CCM3 [*Hack et al., 1998*]. In reality, scavenged dust remains scavenged within hydrometeors until complete evaporation occurs. Thus our evaporative tendency is expected to overestimate the source of dust at lower atmospheric layers in cases where not all precipitation evaporates, i.e., virga. Evaporation is a significant source of dust in some regions. (see Figure 4c).

Cloud aerosol interaction and scavenging are treated using the method of *Rasch et al. [2000]* with modifications. Wet scavenging processes are treated with mass mean, path-normalized scavenging coefficients  $\bar{\Lambda}_M \text{ m}^2 \text{ kg}^{-1}$  defined such that

$$\frac{dM_p}{dt} = -AP_M \bar{\Lambda}_M M_p \quad (23)$$

where  $M_p \text{ kg m}^{-2}$  is the gridcell aerosol mass path,  $A$  is the horizontal fraction of the gridcell over which the scavenging process occurs, and  $P_M \text{ kg m}^{-2} \text{ s}^{-1}$  is the rate of interaction with the scavenging droplets. Nucleation scavenging occurs through the entire vertical domain of the fraction of the gridcell occupied by the appropriate (convective or stratiform) cloud type. For nucleation scavenging,  $P_M$  is the local rate of conversion of water vapor to droplets (condensation) and  $\bar{\Lambda}_M = 0.10$  for all size classes for both stratiform and convective rain. This is identical to the sulfate nucleation scavenging representation of [*Rasch et al., 2000*], except that we allow dust nucleation scavenging in frozen clouds. These modifications to the sulfate scavenging procedure in MATCH are intended to account for the hydrophobic nature of mineral aerosol, as well as its potential role in forming ice nuclei [*Pruppacher and Klett, 1978*]. The present simple formulation of nucleation scavenging must be viewed as a temporary procedure while more microphysically-based methods involving aerosol composition and CCN activation suitable for large scale models are investigated [e.g., *Zhang et al., 2000*].

The treatment of sub-cloud scavenging partially accounts for effects due to vertical cloud structure and to aerosol size and hydrometeor size distribution. For sub-cloud scavenging,  $A$  in (23) is the maximally overlapped fraction of the

**Table 3. Sub-Cloud Scavenging Efficiencies**

Diameter $\mu\text{m}$	Convective		Stratiform	
	Theory <sup>a</sup> $\text{m}^2 \text{kg}^{-1}$	DEAD <sup>b</sup> $\text{m}^2 \text{kg}^{-1}$	Theory $\text{m}^2 \text{kg}^{-1}$	DEAD $\text{m}^2 \text{kg}^{-1}$
0.1–1.0	7.61 – 5	2.00 – 2	2.47 – 4	3.00 – 2
1.0–2.5	4.10 – 3	5.00 – 2	8.53 – 3	1.00 – 1
2.5–5.0	1.05 – 1	1.05 – 1	1.97 – 1	1.97 – 1
5.0–10.0	2.68 – 1	2.68 – 1	4.78 – 1	4.78 – 1

<sup>a</sup>Theoretical values computed as in *Seinfeld and Pandis* [1997]

<sup>b</sup>Value used in DEAD

product of cloud fraction and precipitation rate of all grid-points above the given gridpoint, while  $P_M$  is the appropriate (convective or stratiform) precipitation rate [*Rasch et al.*, 2000]. The model accounts for the strong dependence of sub-cloud scavenging on both the aerosol and precipitation size distributions which arises from the interaction of the constituent processes of Brownian diffusion, interception, and impaction [e.g., *Dana and Hales*, 1976]. The contributions of diffusion, interception, and impaction to the precipitation collection efficiency is modeled following *Seinfeld and Pandis* [1997]. The sub-bin distribution of particles within each transport bin is as described in §2.1. As mentioned above, the transport model separately diagnoses stratiform and convective precipitation. For the purposes of scavenging, stratiform and convective precipitation droplets are assumed to obey lognormal size distributions with number median diameters of 400 and 1000  $\mu\text{m}$ , respectively.

Table 3 shows the wet deposition scavenging efficiencies employed in the model. For each type of precipitation (convective and stratiform are diagnosed separately by MATCH) two below-cloud scavenging efficiencies are shown for each transport bin. The first is a theoretical mass mean scavenging coefficient  $\bar{\Lambda}_M$  and the second is the value DEAD uses. The theoretical  $\bar{\Lambda}_M$  values are obtained using the method of *Dana and Hales* [1976]. The raindrop-aerosol collision efficiency between droplets of size  $D_P$  and dust particles of size  $D_p$  is set to

$$E(D_P, D_p) = E_{BD} + E_{NTC} + E_{MPC} \quad (24)$$

where  $E_{BD}$ ,  $E_{NTC}$ , and  $E_{MPC}$  are the individual collision efficiencies for the processes of Brownian diffusion, interception, and inertial impaction. The meanings and analytic form of each term are given in *Seinfeld and Pandis* [1997]. The collision efficiencies are integrated over the raindrop size distribution and the sub-bin dust distribution. For these calculations, convective and stratiform rain droplets are as-

sumed to adhere to globally uniform lognormal size distributions with number median diameters of 1000 and 400  $\mu\text{m}$ , respectively, and geometric standard deviations of  $\sigma_g = 1.86$ , as in *Dana and Hales* [1976]. The overbar in the  $\bar{\Lambda}_M$  symbol indicates that all of the tabulated efficiencies have been normalized by the precipitation intensity  $P_M \text{kg m}^{-2} \text{s}^{-1}$ . This procedure results  $\bar{\Lambda}_M < 0.01$  for clay-sized dust particles. These small  $\bar{\Lambda}_M$  may be contrasted with empirically determined values of  $\bar{\Lambda}_M$  closer to 0.1 employed in some global models [*Balkanski et al.*, 1993; *Rasch et al.*, 2000].

The  $\bar{\Lambda}_M$  used by DEAD for  $D > 2.5$  were picked to provide more realistic simulations of long-range transported dust. These  $\bar{\Lambda}_M$  are larger than the theoretical values obtained from (24) by a factor of about 200 (for bin 1) and 10 (for bin 2). The extremely small sub-cloud scavenging efficiency of accumulation mode aerosol [see discussion in *Seinfeld and Pandis*, 1997], when applied without modification to dry-sized dust particles in global models, appears to lead to unrealistically long lifetimes. It is possible that dust particles in humid regions are swelled internally (e.g., smectites) [*Pruppacher and Klett*, 1978], coated with water [*Hänel*, 1976], coagulated with other aerosols, or aspherical in shape so that their effective size during transport is larger than accounted for by the model. These mechanisms would increase particle interception and impaction efficiencies in (24) and hence help to reconcile the discrepancy between theoretical and ad hoc values of sub-cloud scavenging efficiencies for  $D < 2.5 \mu\text{m}$  in Table 3. However all these mechanisms except the last also reduce the particle's density which tends to decrease interception and impaction.

### 3. Global Simulations

To evaluate the model predictions against observations, we have simulated the dust distribution for the ten year period 1990–1999 using NCEP/NCAR reanalyses [*Kalnay*, 1996] to drive the DEAD module in the MATCH chemical transport model [*Rasch et al.*, 1997]. The results shown below were obtained from a MATCH run from 19891201–19991231, using 6-hourly NCEP meteorology interpolated to the nearest 30 min. model timestep. Results were archived as daily mean values, then aggregated into monthly, annual, and climatological means. The first month was discarded to remove spin-up effects. We present only the gross climatological simulation of DEAD. We omit discussion of the interannual variability in all but one figure, pending longer model simulations. More extensive comparisons between DEAD and observed dust climatology are shown in *Luo et al.* [2003]; *Mahowald et al.* [2003].

Figure 2 shows the predicted annual mean mobilization and deposition tendencies. In general, entrainment occurs

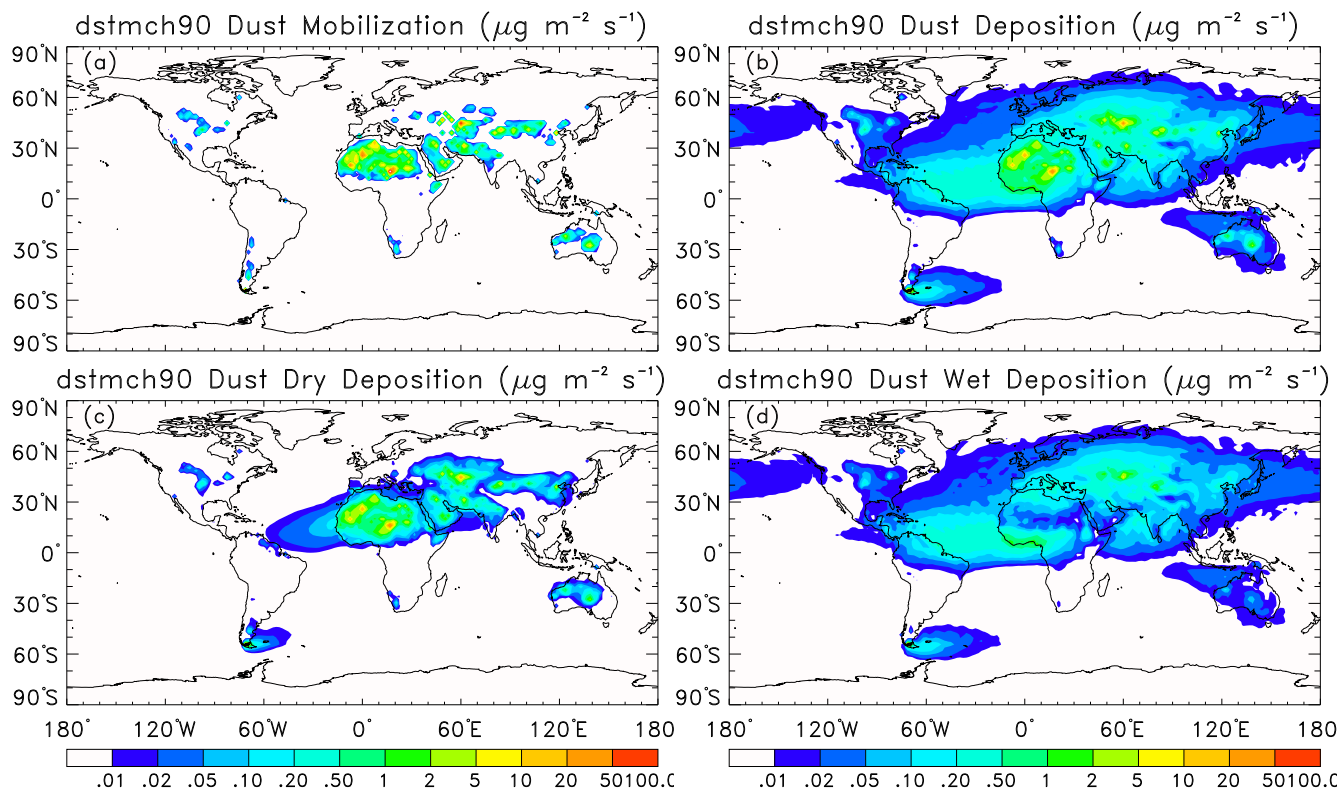


**Figure 2.** Predicted annual mean dust source and sink fluxes in  $\mu\text{g m}^{-2} \text{s}^{-1}$  for (a) mobilization, (b) total deposition, (c) dry deposition, (d) wet deposition. Scale is logarithmic.

in regions with a combination of high winds, low vegetation, no snow cover, and large upstream area. The strongest sources are in North Africa and Asia, consistent with satellite observations and previous studies. [Herman *et al.*, 1997; Husar *et al.*, 1997; Ginoux *et al.*, 2001; Prospero *et al.*, 2002]. These sources include the Bodele depression, Mali and Southern Algeria, the Takli Makan, and Gobi deserts, Patagonia, and the Lake Eyre basin in Australia. North American sources center on Texas and the Great Plains regions, with additional sources in the Sonoran Desert of Mexico and the Southwestern US.

The predicted dust deposition in Figure 2b shows that mass transport affects extensive areas downwind of the source regions. Deposition to the tropical North Atlantic from the North African plume is especially significant, averaging  $750 \text{ mg cm}^{-2} \text{ ka}^{-1}$  in the ocean region bounded by  $0\text{--}30^\circ\text{N}$ ,  $0\text{--}60^\circ\text{W}$ . We estimate an annual mean aeolian deposition flux at the mouth of the Amazon ( $0^\circ\text{N}$ ,  $50^\circ\text{W}$ ) of  $75 \text{ kg ha}^{-1} \text{ yr}^{-1}$ . This is consistent with the estimate by Swap *et al.* [1992] of less than  $190 \text{ kg ha}^{-1} \text{ yr}^{-1}$ .

Figure 2c and d decompose the total deposition into dry and wet deposition fluxes. As expected, dry deposition dom-

inates source regions because of large particle sedimentation. Dry deposition operates continuously, so the dry deposition patterns are an excellent proxy for atmospheric dust loading (Figure 3). Wet deposition removes most dust far from source regions. It accounts for 41% of global deposition, and for 89% of oceanic deposition.

The important role of wet deposition in our study is consistent with some previous modeling studies [Tegen and Fung, 1994; Woodward, 2001] but inconsistent with Ginoux *et al.* [2001], who find that wet deposition accounts for only 13% of global deposition. These models represent wet scavenging differently and use different effective scavenging coefficients. We (Table 3) and Woodward [2001] use size-dependent washout coefficients, while Tegen and Fung [1994], Ginoux *et al.* [2001] and Luo *et al.* [2003] use uniform scavenging coefficients which vary from 250–750. Observations of the ratio of dry to wet deposition are difficult [Duce *et al.*, 1991] and are available at too few locations [e.g., Arimoto *et al.*, 1985; Guieu *et al.*, 1997] to provide robust global constraints. However, spatio-temporal variability in deposition processes would not reconcile the above modeling differences. This emphasizes the need for coordinated,

**Table 4. Oceanic Deposition<sup>a</sup>**

Region	Duce	Prospero	GOCART	DEAD
N. Pacific	480	96	92	31
S. Pacific	39	8	28	8
N. Atlantic	220	220	184	178
S. Atlantic	24	5	20	29
N. Indian	100	20	138	36
S. Indian	44	9	16	12
Global	910	358	478	314

<sup>a</sup>Units are  $\text{Tg yr}^{-1}$ . Sources are *Duce et al.* [1991], *Prospero* [1996b], and *Ginoux et al.* [2001].

long term measurements of the spatial and temporal distribution of wet and dry particle deposition.

In descending order, the annual mean emissions from the relevant continents in  $\text{Tg yr}^{-1}$  are Africa, 980; Asia, 415; Australia, 37; South America, 35; North America, 8. Table 4 compares the predicted annual mean deposition to ocean regions to previous observation-based [*Duce et al.*, 1991; *Prospero*, 1996b] and model [*Ginoux et al.*, 2001] estimates. DEAD and GOCART agree on deposition to the Atlantic and South Indian Oceans, but strongly disagree in the Pacific and North Indian Oceans. The lower estimates of DEAD are much closer than GOCART to *Prospero* [1996b] in the Indian and South Pacific Oceans, but much farther from *Prospero* in the North Pacific. Predicted and observed ocean sediment fluxes from a slightly different version of DEAD, as well as source/sink mappings, are compared in *Luo et al.* [2003].

Table 5 compares the annual mean deposition of trace metals to each ocean. These estimates assume that trace metals constitute a fraction of the dust mass equal to their estimated abundance in the upper continental crust, following *Duce et al.* [1991].

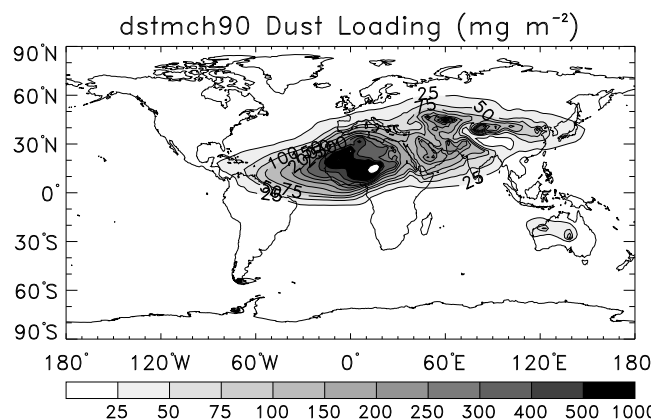
Figure 3 shows the predicted annual mean mass burden in  $\text{mg m}^{-2}$ . Strong dust burdens are apparent over source regions, where large particles have not yet sedimented. Source regions in North and South America and South Africa show no persistent dust burden, contrary to what might be expected based on Figure 2a. Emissions in these mid-latitude source regions are very susceptible to wet scavenging, and so have a relatively short lifetime.

Table 6 compares the climatological (1990–1999) mean budget of the DEAD simulation against previous studies and estimates. DEAD predicts emissions of about  $1490 \text{ Tg yr}^{-1}$  for particles smaller than  $10 \mu\text{m}$ . This is about 84% of the

**Table 5. Trace Metal Deposition to Oceans<sup>a</sup>**

Region	Al	Fe	Si	P
N. Pacific	2.5	1.1	9.7	0.03
S. Pacific	0.7	0.3	2.6	0.01
N. Atlantic	14.3	6.2	55	0.19
S. Atlantic	2.3	1.0	8.9	0.03
N. Indian	2.9	1.3	11.1	0.04
S. Indian	0.9	0.4	3.6	0.01
Global	25.3	11.0	96.8	0.33

<sup>a</sup>Units are  $\text{Tg yr}^{-1}$ . Assumes dust is 8.01% Al, 3.5% Fe, 30.8% Si, and 1050 ppm P as in *Duce et al.* [1991].



**Figure 3.** Predicted annual mean dust mass burden in  $\text{mg m}^{-2}$ . Scale is non-linear.

**Table 6. Climatological Budget Statistics<sup>a b</sup>**

Quantity	Andreae	Tegen	GOCART <sup>c</sup>	DEAD
Emission	1500	1222	1814	1490
Lifetime	4	4	7.1	4.3
Burden	8.4	18.8	35.9	17.4
$\tau$ Ocean	—	—	—	0.020
$\tau$ Land	—	—	—	0.051
$\tau$ Global	0.023	0.033	—	0.030

<sup>a</sup>Emission in  $\text{Tg yr}^{-1}$ , Lifetime in days, Burden in  $\text{Tg}$ , Optical depths  $\tau$  at  $0.63 \mu\text{m}$ .

<sup>b</sup>Sources: *Andreae* [1996], *Tegen and Fung* [1994], *Ginoux et al.* [2001]

<sup>c</sup>For size range  $0.2 \leq D \leq 12 \mu\text{m}$

GOCART estimate of  $1782 \text{ Tg yr}^{-1}$  for  $D < 12 \mu\text{m}$  [Ginoux *et al.*, 2001]. The reduced emissions predicted by DEAD relative to GOCART are consistent with the relative dust concentrations and deposition fluxes (and their biases) predicted by the models. DEAD is consistent with the IPCC estimate of the range of  $D < 20 \mu\text{m}$  dust emissions in the year 2000 of  $1000\text{--}3000 \text{ Tg yr}^{-1}$  with a best guess value of  $2150 \text{ Tg yr}^{-1}$  [Penner *et al.*, 2001].

Due to the relatively short length of our base simulation (1990–1999) we have not until now discussed the modeled interannual dust variability. To illustrate this we computed the modeled mean  $\bar{x}$  and interannual variability for dust emissions, burden and optical depth from the 10 total years (1990–1999). We quantify the interannual variability using the standard deviation  $\sigma_x$  of the global annual mean timeseries of each field. The resulting estimates of  $\bar{x} \pm \sigma_x$  for the 1990s are: Emissions,  $1490 \pm 160 \text{ Tg yr}^{-1}$ ; Burden,  $17 \pm 2 \text{ Tg}$ ; Optical depth,  $0.030 \pm 0.004$ . The normalized variability ( $\sigma_x/\bar{x}$ ) is 10–15% for all three fields. The normalized variability in emission is slightly less than that for burden and optical depth because emission is sensitive to all particle sizes (see Table 8 below), whereas burden and optical depth are not sensitive to the largest particle sizes. Interestingly, the 1996–1998 means were all about 20% less dusty than 1990–1995.

Figure 4 shows the predicted annual mean mixing ratio and source and sink tendencies. Figure 4a shows maxima in the subtropical belts which contain the Earth’s major desert sources. Dust from North Africa and the Saudi Arabian peninsula dominates the northern hemisphere zonal mean. The broad half-width of the maxima is due to the inclusion of central and east Asian dust sources which are  $5\text{--}10^\circ$  north of the African sources. Australia and Patagonian sources create the peak in the southern hemisphere. Figure 4b shows that northern hemispheric wet deposition occurs in two distinct meridional locations: scavenging over the Atlantic and Indian Oceans accounts for the subtropical maxima, while scavenging over the Pacific determines the extratropical maxima.

As mentioned in Section 2.9, stratiform rain continually releases scavenged dust in proportion to its local evaporation rate. Figure 4c shows that gravitational settling is about 5–10 times less efficient than wet processes in removing dust from the free atmosphere in the subtropics. Settling is a small source of dust at low levels near the equator and in the extratropics and in the polar regions. Turbulent deposition operates only in the lowest model layer and thus is difficult to portray in vertical cross-section (see Figure 2c for turbulent deposition). Figure 4d shows that evaporation of stratiform rain vertically redistributes a significant fraction of the scavenged dust. Evaporation is comparable to wet scavenging

**Table 7. Global mean turnover time (days) by removal process**

Diameter	Grav	Turb	Dry	Wet	Total
0.1–1.0 $\mu\text{m}$	1059	928	494	18	17
1.0–2.5 $\mu\text{m}$	171	198	92	12	11
2.5–5.0 $\mu\text{m}$	34	7	6	9	3.5
5.0–10.0 $\mu\text{m}$	7	1.6	1.3	6.1	1.1
0.1–10.0 $\mu\text{m}$	40	9.1	7.4	10.5	4.3

**Table 8. Global Emissions and Deposition Fluxes**

Diameter $\mu\text{m}$	Source $\text{Tg yr}^{-1}$	Dry $\text{Tg yr}^{-1}$	Wet $\text{Tg yr}^{-1}$	Load $\text{Tg}$	Life day
0.1–1.0	48	2	47	2.2	17
1.0–2.5	260	31	229	7.7	11
2.5–5.0	609	371	236	5.8	3.5
5.0–10.0	573	463	96	1.6	1.1
0.1–10.0	1490	866	607	17.4	4.3

over the tropical North Atlantic. A more complex but physically consistent model representation of evaporation would release scavenged dust discretely as each rain droplet completely evaporated, i.e., in *virga*. Thus it is likely our model overestimates the importance of evaporation.

Table 7 shows the size dependence of all deposition timescales in days. Dry deposition is the sum of Gravitational and Turbulent deposition. The turnover time for particles in the accumulation mode ( $D < 2.5 \mu\text{m}$ ) is order months when considering only dry processes. The relative importance of dry and wet deposition changes at  $2.5 \mu\text{m}$ , near the boundary between clay and silt-sized particles. Wet scavenging accounts for 41% of global mean deposition and dry processes account for 59%. The size dependent global annual mean fluxes are summarized in Table 8. Wet deposition is the only effective removal process for small particles in our model. This is consistent with some *Teegen and Fung* [1994], but not all [Ginoux *et al.*, 2001] previous studies.

We compare the predicted Aerosol Optical Depth (AOD) at  $0.63 \mu\text{m}$  against AOD inferred from AVHRR channel 1 observations [Stowe *et al.*, 1997] with a nominal band center of  $0.63 \mu\text{m}$ . Table 2 lists the specific extinction coefficients used for each bin. Figure 5 shows the predicted seasonal mean dust optical depth at  $0.63 \mu\text{m}$ . This figure may be compared to Husar *et al.* [1997], Figure 1. Note the scale is non-linear for  $\tau > 0.5$ . The seasonal migration of the North African dust plume with the ITCZ seen in AVHRR and TOMS observations [Husar *et al.*, 1997; Herman *et al.*,

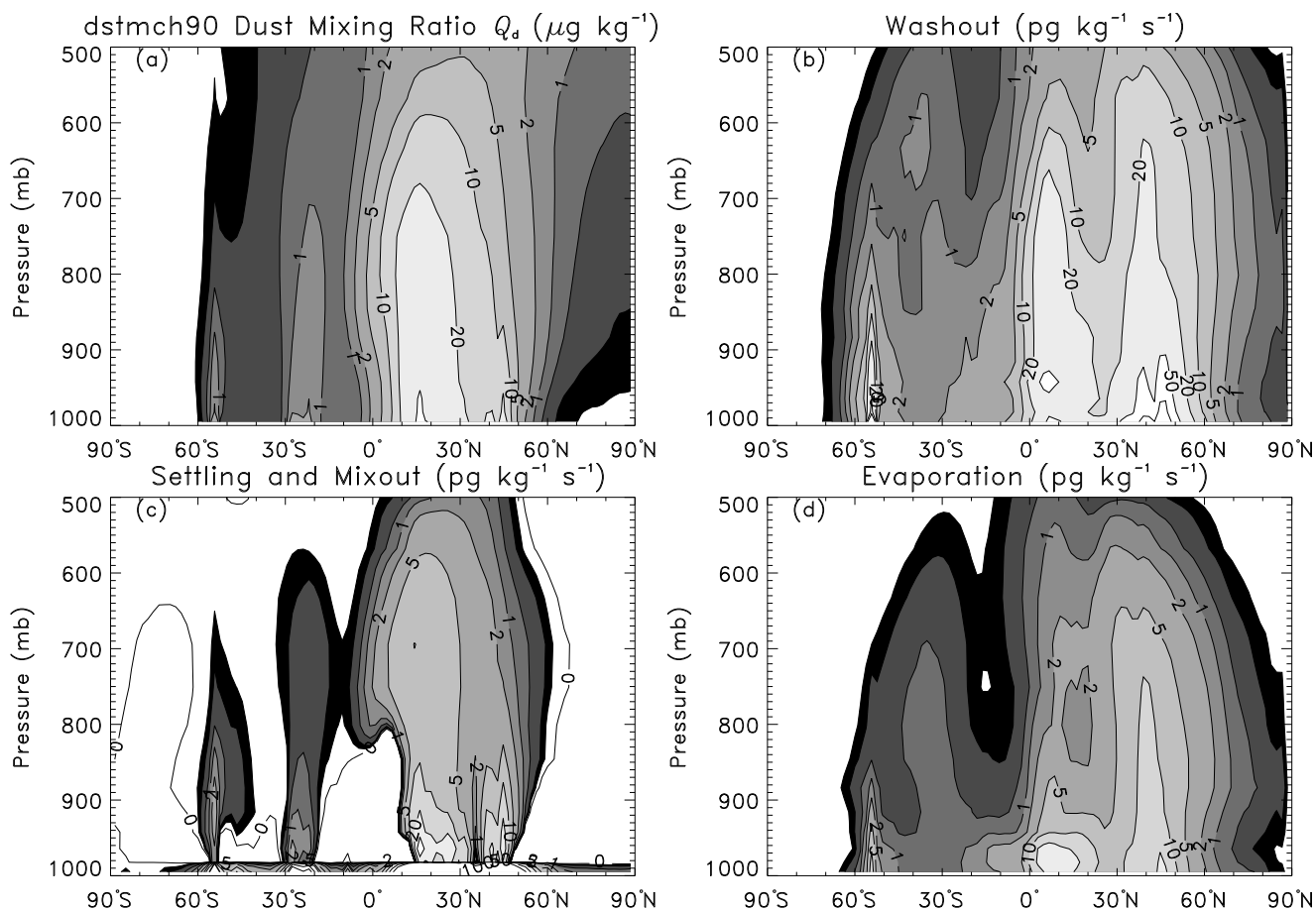


**Figure 4.** Predicted climatological mean dust mixing ratio and mixing ratio tendencies. Shown are (a) mixing ratio in  $\mu\text{g kg}^{-1}$ , and, in  $\text{pg kg}^{-1} \text{s}^{-1}$ , (b) wet deposition, (c) dry deposition, and (d) evaporation. Contour intervals are logarithmic.

1997], and in other models [Tegen and Fung, 1995; Ginoux et al., 2001; Luo et al., 2003], is clearly present. This dust plume is thought to dominate the AVHRR observed total aerosol plume in July, and to contribute about half of the observed optical depth in January, when it is complemented by carbonaceous aerosol from biomass burning [Chin et al., 2002]. The dust plume reaches its farthest westward extent in July, when it is observed to be responsible for the majority of aerosol scattering as far north as Miami [Prospero, 1999]. The peak extent of the Asian-Pacific dust plume occurs in northern Spring. Vertical cross-sections of the seasonal dust distribution (not shown) reveal that East Asian dust may travel 200 mb higher in the atmosphere than African dust.

#### 4. Station-based Evaluations

Surface observations at sites managed by the University of Miami provide a unique long-term record and climatology

of surface dust concentrations. The dust concentration data (which are provided by J. Prospero and D. Savoie) for many U. Miami stations are calculated from Al concentrations provided by R. Arimoto. Interannual and decadal trends in the African dust plume in the North Atlantic have been analyzed using these data [e.g., Prospero and Nees, 1986; Prospero, 1996a]. Previous global dust simulations have been evaluated against these U. Miami station observations [Tegen and Fung, 1994; Tegen et al., 1996; Mahowald et al., 1999; Ginoux et al., 2001; Perlwitz et al., 2001; Luo et al., 2003; Penner et al., 2001]. Station locations [Ginoux et al., 2001; Woodward, 2001] and sampling techniques [Savoie et al., 1992; Maring et al., 2000] are discussed in the literature. Figure 6 compares predicted to observed monthly mean dust concentrations in  $\mu\text{g m}^{-3}$ . All stations are compared to 1990–1999 model climatology except Sal Island, Jeju (formerly known as Cheju), Okinawa, and Mace Head. Model data for these stations were sub-sampled to include

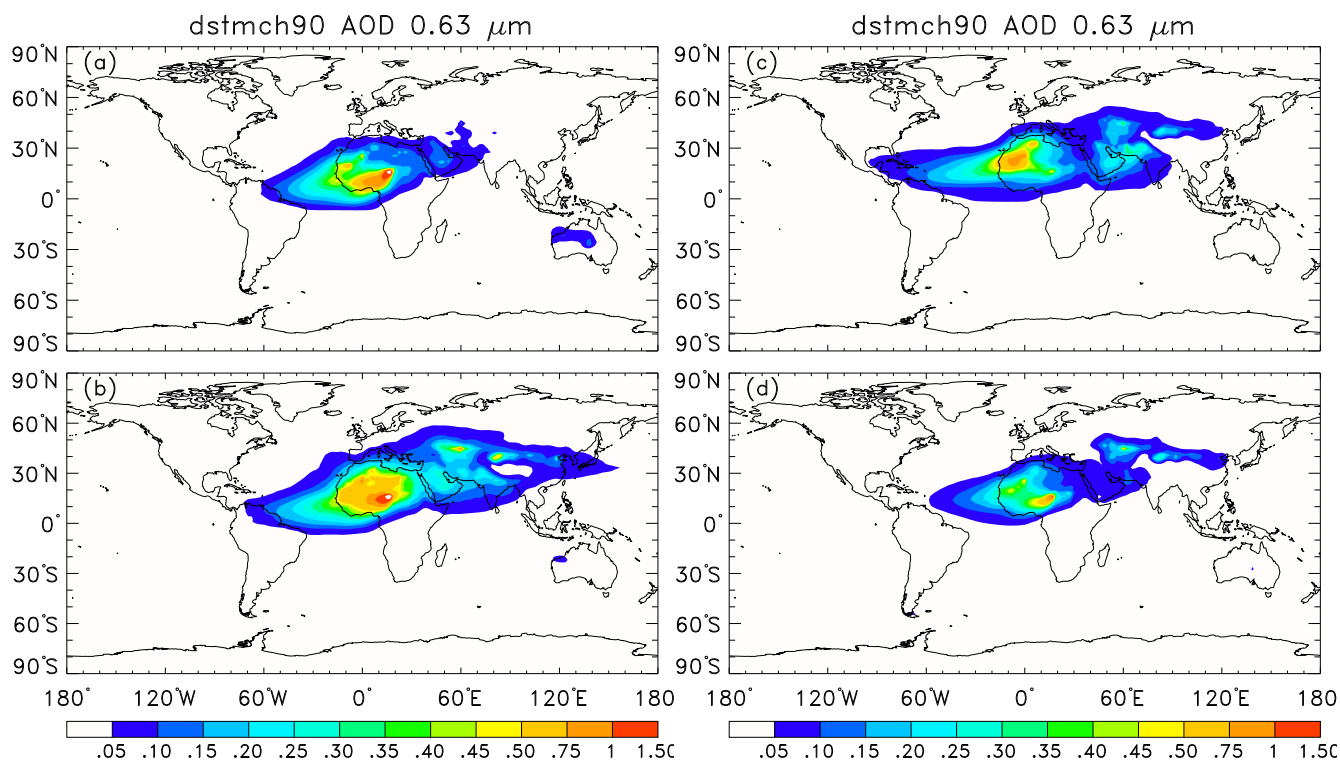


**Figure 5.** Predicted seasonal mean dust optical depth at 0.63 μm for (a) DJF, (b) MAM, (c) JJA, and (d) SON.

only months during which observations were recorded.

The first six stations are sensitive to the North African dust plume. The modeled and observed surface dust seasonal cycle generally overlap at Barbados, Miami, Bermuda, Izaña, Sal Island and Mace Head. At Barbados, the observed seasonal cycle peaks in June but DEAD peaks in May and is too active in winter. In Miami and Bermuda the peak occurs in July and August in both observed and model results, but the modeled amplitude appears too weak in summer. In general the phasing and amplitude of the surface concentration is within the monthly variance at these stations. We are currently producing longer model climatologies to better quantify the model variance. The greatest absolute disparity with the North Atlantic measurements occurs in the winter at Sal Island, about 700 km from the African continent, when the model overpredicts dust concentration by a factor of two. This disparity indicates a problem with source regions near the coast or the vertical location of the plume. Izaña, which lies only 350 km from Western Sahara coast, and is located at 2360 m in the free troposphere, is also overpredicted in amplitude, but only by 20%. At Izaña, however, the observational sampling is sectorized to the west, and so may miss some large dust events which could help to reconcile the model and measurements. The simulation at Mace

Head has a low annual-mean concentration with strong variability in springtime as observed.

Evaluating the dust distribution over the Indian Ocean is difficult due to the paucity of data there [Prospero, 1996b]. The seasonal cycle at Kaashidhoo appears reasonable, but anthropogenic aerosol such as fly ash may account for a significant fraction of the aerosol reported as dust (D. Savoie, personal communication, 1999). Thus DEAD's underestimate of concentration at Kaashidhoo may be more representative of true desert dust in the central Indian Ocean region.

Station observations in the North Pacific generally show a springtime concentration maximum [Prospero, 1996b]. DEAD captures this seasonal phasing at Jeju, Okinawa, Enewetak, and Midway. The observed and modeled climatology at Oahu are very similar to Midway and have been omitted. DEAD underestimates the mean concentrations closer to the Asian sources at Jeju and Okinawa (where complex terrain may bias sampling) by about 40%, with most of the bias occurring during the winter and spring. On the other hand, DEAD overestimates concentrations farther from the continent at Enewetak, Midway and Oahu by up to 100%, most noticeably in spring. Excessive springtime transport of African dust contributes to this high bias.

The South Pacific stations farthest from source regions

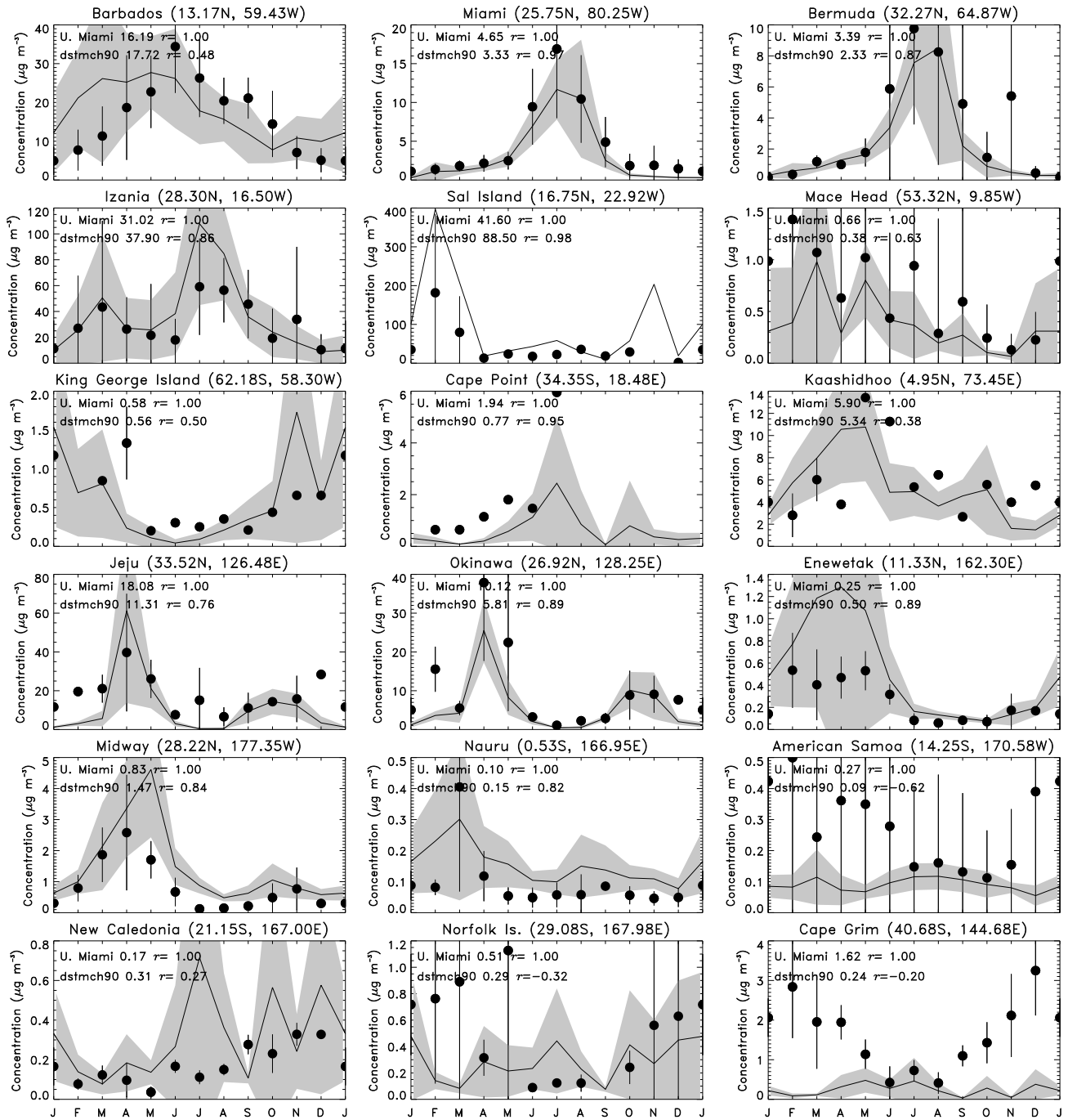


**Figure 6.** Predicted (line) and observed (circles) monthly mean surface dust concentration ( $\mu\text{g m}^{-3}$ ) at U. Miami stations. Two standard deviations are shown for predicted (shading) and observed (whiskers) values. No whisker indicates data only available for same month in  $N < 2$  years. Station and model names are followed by the climatological mean concentration ( $\mu\text{g m}^{-3}$ ) and the linear correlation coefficient  $r$  with the observed monthly mean data.

show weak seasonal cycles and very low mean concentrations. The overlap between U. Miami observations and

model predictions is generally acceptable at Nauru, American Samoa, and New Caledonia. Cape Grim, however,

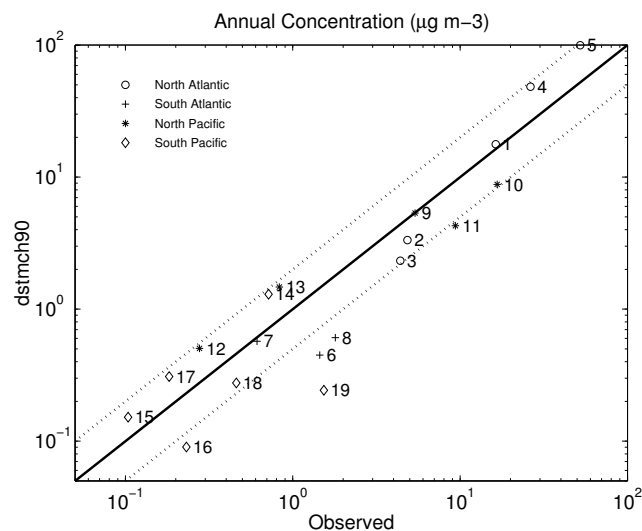


**Figure 7.** Predicted and observed climatological mean surface concentration of dust in  $\mu\text{g m}^{-3}$  at U. Miami stations. Dashed lines indicate factor of two disparity. Site numbers are 1. Barbados, 2. Miami, 3. Bermuda, 4. Izaña, 5. Sal Island, 6. Mace Head, 7. King George Island, 8. Cape Point, 9. Kaashidhoo, 10. Jeju, 11. Okinawa, 12. Enewetak, 13. Midway, 14. Oahu, 15. Nauru, 16. American Samoa, 17. New Caledonia, 18. Norfolk Island, 19. Cape Grim.

which is closest to a source region (Australia), shows a strong austral summer peak in the observations that is absent in the model. Closer examination (see, e.g., Figure 2a,b and Figure 5a) shows that DEAD captures the phasing of summertime Australian emissions, but that the circulation moves this dust more efficiently toward the northwest than the southeast to Cape Grim.

Intercomparison of model performance among all the U. Miami-operated stations shows the great dynamic range of dust concentration in the atmosphere. The climatological mean observed and modeled concentrations at each station in Figure 6 are scatter-plotted in Figure 7. Both observed and modeled concentrations span three orders of magnitude. In general, stations downwind of the African plume are better simulated than Asian and North Pacific stations which are in turn better simulated than southern hemisphere stations. Disparities at stations with the highest and lowest mean dust concentrations are generally less than a factor of two, and the model is never more than a factor of two too high. Dust concentration appears significantly underpredicted at four stations in the southern hemisphere: American Samoa, Cape Point, Cape Grim, and Norfolk Island. Simulations at the latter three stations suggest inadequate emissions and transport from South Africa and from Australia, respectively. How-

ever, Cape Point and Cape Grim measurements may be biased by the complex terrain surrounding the stations. In general, local sources cause relatively more severe contamination of samples at stations with very low dust concentration, such as those in the southern hemisphere (J. Prospero, personal communication, 2002).

Low concentrations at Jeju and Okinawa suggest a too weak source upwind in the Takli Makan and Gobi deserts. We appear to underpredict dust at Mace Head similar to Woodward [2001] but opposite to Ginoux *et al.* [2001]. This suggests inadequate transport from North African sources, but the high variability emphasizes the importance of obtaining lengthier simulations and measurements.

Long term land-based measurements of deposition fluxes are highly valuable for model evaluation since, unlike marine sediments, they reflect only atmospheric transport and can be precisely dated. Ginoux *et al.* [2001] compiled observations previously reported in the literature from 11 locations which span both hemispheres and approximately 90-station-years of measurements from the 1950s to the present. The majority of the stations were most active in the 1980s, before our simulation period. Comparisons to deposition at Shemya, Nauru, New Caledonia, Rarotonga, and Norfolk Island are not possible because only concentration was measured at these stations. The deposition measurements used in Ginoux *et al.* [2001] for these 5 stations were based on a misinterpretation of this point. Figure 8 compares our 1990-1999 mean predictions with the 11 stations in this observed climatology. A model low bias is readily apparent at land locations in Asia and at most ocean locations. No consistent trend is apparent at the stations which sample the North African plume. Mean deposition appears high in the French Alps, somewhat low in Spain, and good in Miami. Mean deposition is underpredicted by more than a factor of two at both Asian land stations, Taklimakan and Tel Aviv. Since these stations are near active source regions, underpredictions there, similar to Ginoux *et al.* [2001], could result from neglecting transport of  $D > 10 \mu\text{m}$  particles or missing small but nearby sources.

Comparisons at Pacific stations are mixed but a low bias is evident. Mean deposition appears significantly low at Midway and Oahu in the North Pacific, although Shemya in the western Aleutians is well simulated. Simulated deposition is also low in the equatorial Pacific at Enewetak, Nauru, and Samoa, but not at Fanning. Finally in the South Pacific simulated deposition appears too low at Rarotonga, New Caledonia, and Norfolk, but not at New Zealand. The Pacific stations are generally far from emissions and so integrate deposition fluxes over large regions. Low model deposition fluxes there indicate a bias in transport and removal of smaller particles. This low bias is consistent with excessive

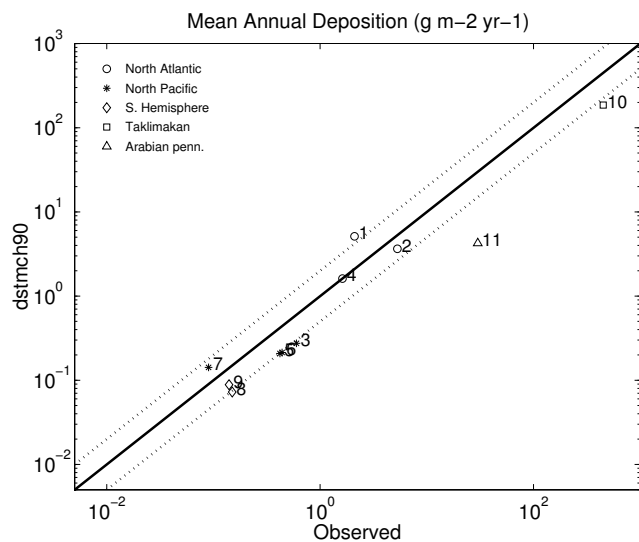


**Figure 8.** Predicted and observed climatological mean dust deposition flux dust in  $\text{g m}^{-2} \text{yr}^{-1}$  at 11 stations compiled by [Ginoux et al. \[2001\]](#). Site numbers are 1. French Alps (45.5N, 6.5E), 2. Spain (41.8N, 2.3E), 3. Midway (28.2N, 177.35W), 4. Miami (25.75N, 80.25W), 5. Oahu (21.3N, 157.6W), 6. Enewetak (11.3N, 162.3E), 7. Fanning (3.9N, 159.3W), 8. Samoa (14.25S, 170.6W), 9. New Zealand (34.5S, 172.75E), 10. Taklimakan (40.0N, 85.0E), 11. Tel Aviv (32.0N, 34.5E).

wet scavenging upstream and/or insufficient turbulent mix-out at the surface. However, the mismatch between simulation and observation periods may contribute significantly to the apparent magnitude of the low bias.

In summary, the model performs much better in terms of surface concentrations than deposition fluxes. The model tendency to underestimate the full amplitude of the seasonal cycle of dust concentration at key stations downwind of North Africa (Barbados), East Asia (Jeju), and Australia (Cape Grim) suggests biases in model emissions. The inclusion of anthropogenic dust sources could help remediate these biases, if such sources were known. The model tendency to underestimate deposition fluxes in remote regions of the Pacific is more indicative of biases in small particle transport and scavenging mechanisms.

## 5. Discussion and Summary

The basis of a physical model for global dust entrainment and deposition, DEAD, has been described. Entrainment is based on saltation theory adjusted to fit wind tunnel measurements. The soil erodibility is proportional to the runoff area upstream of each source region. Deposition is

determined by size resolved particle and precipitation aerodynamics. We prescribe only a minimal set of ad hoc corrections to physical processes and do not invoke any anthropogenic emissions. The main features of a model climatology generated from a 1990–1999 simulation were presented. The spatial and temporal patterns of the atmospheric dust are consistent with station observations and satellite imagery on this timescale. The credibility of the simulations produced by this factor support the hypothesis that dust emission “hot spots” exist in regions where alluvial sediments accumulate and may be disturbed [[Herman et al., 1997](#); [Gillette, 1999](#); [Prospero et al., 2002](#)]. This naturally determined erodibility factor helps to constrain the role anthropogenic dust may play in present climate.

Based on simulations of 1990–1999, we estimate the global annual mean and variability of  $D < 10 \mu\text{m}$  dust to be: Emissions,  $1490 \pm 160 \text{ Tg yr}^{-1}$ ; Burden,  $17 \pm 2 \text{ Tg}$ ; Optical depth at  $0.63 \mu\text{m}$ ,  $0.030 \pm 0.004$ . For comparison, DEAD predicts about 80% of the emissions, 60% of the lifetime, and only 45% of the burden predicted by GOCART [[Ginoux et al., 2001](#)], which uses a distinct set of physical parameterizations and analyzed winds. Clearly the sensitivity of model predictions to analyzed meteorologies and model resolution should be investigated before drawing firm conclusions regarding the contribution of model physics to climatological biases. However, the differences between DEAD and observations and other models do suggest possible causes of the model biases and their potential improvements.

As mentioned earlier, recent measurements from the PRIDE experiment [[Reid et al., 2003](#)] show that the transport mode of African dust is about  $\bar{D}_v = 3.5 \mu\text{m}$  or larger. This is significantly greater than the  $\bar{D}_v = 2.5 \mu\text{m}$  predicted by DEAD in the Caribbean (Figure 1) and used for our sub-bin distribution (Table 2). A larger transport mode could help to reconcile some of the disparities between DEAD and observations. In particular, a larger  $\bar{D}_v$  would allow predicted optical depths to remain constant or decrease at the same time as mass concentrations and thus deposition fluxes increase. Understanding the physical processes which permit efficient transport of particles coarser than the accumulation mode is a key problem for future studies. These processes may include particle size at the source, particle shape, particle density, and numerical representation of advection.

DEAD treats convective and stratiform nucleation and collection scavenging using a relatively sophisticated size-resolved technique. Collection by convective precipitation and nucleation scavenging by stratiform precipitation are extremely important as these processes determine the lifetime of long range transported dust in our model. Although successful in many regions, this treatment does not yet capture the full phasing and amplitude of the seasonal cycle of

dust over the sub-tropical north Atlantic, so further improvements are required. The relative roles of wet and dry deposition vary dramatically among models [Ginoux *et al.*, 2001]. However, the physical parameters which control wet scavenging are not amenable to measurement. Near-term improvements of in-cloud and below cloud scavenging, therefore, may continue to depend on iteratively refining models against observables such as concentration and optical depth.

The DEAD model has many limitations. The mobilization parameterization is detailed yet still omits some important processes. Factors known to have a significant influence on dust emissions which are not directly accounted for in the present model include: geographic variation of surface size distributions [Marticorena *et al.*, 1997], soil modulus of rupture [Gillette, 1988], binding by plant root matter, spacing and aspect ratio of non-erodible roughness elements [Rau-pach, 1994], size-dependent energy thresholds for particle release during sandblasting [Lu and Shao, 1999; Alfaro and Gomes, 2001]. Because of the absence of these processes, the present model is one of intermediate complexity. Where warranted, these limitations may be addressed by more realistic (and expensive) physical representations. We are now testing a refined saltation-sandblasting model [Grini *et al.*, 2002] which predicts rather than prescribes the source size distribution. We are also using DEAD in CTMs to understand aerosol composition, transport, and radiative forcing during the PRIDE and ACE-Asia experiments.

Some current constraints in DEAD are assumptions which will be re-examined when adequate or improved boundary data become available in the host model. Examples include accounting for spatial heterogeneity in the smooth roughness length (2), tightening the relatively weak moisture inhibition (6), and relaxing ad hoc constraints on emissions north of 60°N. However, our initial results show that an intermediate complexity model is capable of reproducing many features of the dust distribution observed in the current climate.

The DEAD model and this climatology are available to all interested researchers. Visit the model homepage (<http://dust.ess.uci.edu/dead>) or contact the authors for details. DEAD also runs as a standalone box model for convenient calibration against station or wind-tunnel measurements of erosion. DEAD has been integrated into a general circulation model (GCM), the National Center for Atmospheric Research Community Climate Model version 3. Future studies employing DEAD in GCMs will evaluate the radiative forcing due to dust, and associated climate feedback of both the atmosphere and coupled climate systems.

The DEAD model was designed to be physically based as much as possible. The wide range of spatial and temporal scales involved in global dust production necessitated some tuning of the parametric relations which were mainly

derived from wind tunnel measurements. Nevertheless, the response of dust production and transport to many key climate and landscape parameters has been included. Thus DEAD should be suitable for studies of the interaction between dust and climate change in past, present, and future climates. Currently DEAD is being used to investigate dust radiative forcing and feedback in the present climate, oxidant uptake and photochemistry, the roles of atmospheric iron and silica in marine productivity. DEAD has been built upon the physics of natural erosion so that anthropogenic dust sources are not yet explicitly represented. In the future we hope to identify and explicitly include anthropogenic dust sources.

**Acknowledgments.** CSZ thanks R. Arimoto, P. Ginoux, J. Herman, K. Kohfeld, C. Luo, N. Mahowald, J. Prospero, D. Savoie, I. Sokolik, L. Stowe, O. Torres, and two anonymous reviewers for providing data and suggestions to evaluate and improve the model, often prior to publication, and for helpful comments. J. Famiglietti, S. Levis, and P. Rasch provided helpful guidance with hydrologic algorithms, land surface characteristics, and aerosol parameterization, respectively. G. Brasseur, J. Kiehl, and the NCAR ASP program provided support and encouragement. This research was supported in part by NASA Grants NAG5-10147 and NAG5-10546.

## References

- Alfaro, S. C., and L. Gomes, Modeling mineral aerosol production by wind erosion: Emission intensities and aerosol size distributions in source areas, *J. Geophys. Res.*, 106(D16), 18,075–18,084, 2001. 2.1, 2.3, 5
- Alfaro, S. C., A. Gaudichet, L. Gomes, and M. Maillé, Modeling the size distribution of a soil aerosol produced by sandblasting, *J. Geophys. Res.*, 102(D10), 11,239–11,249, 1997. 2.3
- Andreae, M. O., Climatic effects of changing atmospheric aerosol levels, in *Future Climates of the World: A Modelling Perspective, World Survey of Climatology*, vol. 16, edited by A. Henderson-Sellers, pp. 347–398, Elsevier, Amsterdam, 1996. b
- Arimoto, R., R. A. Duce, B. J. Ray, A. D. Hewitt, and J. Williams, Atmospheric trace elements at Enewetak Atoll, 2, Transport to the ocean by wet and dry deposition, *J. Geophys. Res.*, 90, 2391–2408, 1985. 3
- Bagnold, R. A., *The Physics of Blown Sand and Desert Dunes*, Methuen & Co. Ltd., London, 1941. 2.2
- Balkanski, Y. J., D. J. Jacob, G. M. Gardner, W. C. Graustein, and K. K. Turekian, Transport and residence times of tropospheric aerosols inferred from a global three-dimensional simulation of <sup>210</sup>Pb, *J. Geophys. Res.*, 98(D11), 20,573–20,586, 1993. 2.9
- Batt, R. G., and S. A. Peabody II, Threshold friction velocities for large pebble gravel beds, *J. Geophys. Res.*, 104(D20), 24,273–24,279, 1999. 2.2
- Belly, P. Y., Sand movement by wind, *Technical Memorandum 1*, US Army Coastal Engineering Research Center, 1964. 2.2
- Bonan, G. B., A land surface model (LSM version 1.0) for ecological, hydrological, and atmospheric studies: Technical descrip-

- tion and user's guide, *Tech. Rep. NCARTN-417+STR*, National Center for Atmospheric Research, Boulder, Colo., 1996. 2.1, 2.2, 2.6, 2.6, 2.8.2
- Bonan, G. B., S. Levis, L. Kergoat, and K. W. Oleson, Landscapes as patches of plant functional types: An integrating concept for climate and ecosystem models, *In press in Global Biogeochem. Cycles*, 2002. 2.6
- Chin, M., et al., Tropospheric aerosol optical thickness from the GOCART model and comparisons with satellite and sun photometer measurements, *J. Atmos. Sci.*, 59(3), 461–483, 2002. 3
- Cogley, J. G., Global hydrographic data release 2.0, *Climate Note 91-1*, Dept. of Geography, Trent University, Peterborough, Ontario, Canada, 1991. 2.6
- Collins, W. D., P. J. Rasch, B. E. Eaton, B. Khattatov, J.-F. Lamarque, and C. S. Zender, Forecasting aerosols using a chemical transport model with assimilation of satellite aerosol retrievals: Methodology for INDOEX, *J. Geophys. Res.*, 106(D7), 7313–7336, 2001. 1
- Collins, W. D., P. J. Rasch, B. E. Eaton, D. W. Fillmore, J. T. Kiehl, C. T. Beck, and C. S. Zender, Simulation of aerosol distributions and radiative forcing for INDOEX: Regional climate impacts, *J. Geophys. Res.*, 107(D19), 8028, doi:10.1029/2000JD000,032, 2002. 1
- D'Almeida, G. A., On the variability of desert aerosol radiative characteristics, *J. Geophys. Res.*, 92, 3017–3026, 1987. 2.4, a
- Dana, M. T., and J. M. Hales, Statistical aspects of the washout of polydisperse aerosols, *Atmos. Environ.*, 10, 44–50, 1976. 2.9, 2.9, 2.9
- Dentener, F. J., G. R. Carmichael, Y. Zhang, J. Lelieveld, and P. J. Crutzen, Role of mineral aerosol as a reactive surface in the global troposphere, *J. Geophys. Res.*, 101(D17), 22,869–22,889, 1996. 2.5
- Duce, R. A., et al., The atmospheric input of trace species to the world ocean, *Global Biogeochem. Cyc.*, 5(3), 193–259, 1991. 3, a, 3, a
- Fécan, F., B. Marticorena, and G. Bergametti, Parametrization of the increase of the aeolian erosion threshold wind friction velocity due to soil moisture for arid and semi-arid areas, *Annales Geophysicae*, 17, 149–157, 1999. 2.2, 2.2
- Genthon, C., Simulations of desert dust and sea-salt aerosols in Antarctica with a general circulation model of the atmosphere, *Tellus*, 44B(4), 371–389, 1992. 2.3
- Gillette, D. A., Threshold friction velocities for dust production for agricultural soils, *J. Geophys. Res.*, 93(D10), 12,645–12,662, 1988. 2.2, 5
- Gillette, D. A., A qualitative geophysical explanation for “hot spot” dust emitting source regions, *Contr. Atmos. Phys.*, 72(1), 67–77, 1999. 2.6, 5
- Gillette, D. A., E. Hardebeck, and J. Parker, Large-scale variability of wind erosion mass flux rates at Owens Lake 2. Role of roughness change, particle limitation, change of threshold friction velocity, and the Owen effect, *J. Geophys. Res.*, 102(D22), 25,989–25,998, 1997. 2.1
- Gillette, D. A., B. Marticorena, and G. Bergametti, Change in the aerodynamic roughness height by saltating grains: Experimental assessment, test of theory, and operational parameterization, *J. Geophys. Res.*, 103(D6), 6203–6209, 1998. 2.2
- Ginoux, P., M. Chin, I. Tegen, J. Prospero, B. Holben, O. Dubovik, and S.-J. Lin, Sources and distributions of dust aerosols simulated with the GOCART model, *J. Geophys. Res.*, 106(D17), 20,555–20,273, 2001. 1, 2.3, 2.6, 3, a, b, 3, 3, 3, 4, 4, 4, 8, 5
- Global Soil Data Task, *Spatial Database of Soil Properties*, International Geosphere-Biosphere Programme - Data and Information System, Toulouse, France, 1999. 2.2, 2.3
- Gomes, L., G. Bergametti, G. Coudé-Gaussen, and P. Rognon, Submicron desert dusts: A sandblasting process, *J. Geophys. Res.*, 95(D9), 13,927–13,935, 1990. 2.3
- Greeley, R., and J. D. Iversen, *Wind as a geological process*, no. 4 in Cambridge Planetary Science Series, Cambridge Univ. Press, New York, NY, 1985. 2.2, 2.3
- Grini, A., C. S. Zender, and P. Colarco, Saltation sandblasting behavior during mineral dust aerosol production, *Geophys. Res. Lett.*, 29(18), 1868, doi:10.1029/2002GL015,248, 2002. 2.1, 2.3, 2.3, 5
- Guieu, C., R. Chester, M. Nimmo, J. M. Martin, S. Guerzoni, E. Nicolas, J. mateu, and S. Keyse, Atmospheric input of dissolved and particulate metals to the northwestern Mediterranean, *Deep-Sea Research II*, 44, 655–674, 1997. 3
- Hack, J. J., Parameterization of moist convection in the National Center for Atmospheric Research community climate model (CCM2), *J. Geophys. Res.*, 99(D3), 5551–5568, 1994. 2
- Hack, J. J., J. T. Kiehl, and J. W. Hurrell, The hydrologic and thermodynamic characteristics of the NCAR CCM3, *J. Clim.*, 11(6), 1151–1178, 1998. 2.9
- Hänel, G., The properties of atmospheric aerosol particles as functions of the relative humidity at thermodynamic equilibrium with the surrounding moist air, *Adv. Geophys.*, 19, 73–188, 1976. 2.9
- Herman, J. R., P. K. Bhartia, O. Torres, C. Hsu, C. Seftor, and E. Celarier, Global distribution of UV-absorbing aerosols from Nimbus 7/TOMS data, *J. Geophys. Res.*, 102(D14), 16,911–16,922, 1997. 2.6, 3, 3, 5
- Hillel, D., *Introduction to Soil Physics*, Academic Press, San Diego CA, 1982. 2.6
- Holben et al., B. N., AERONET – a federated instrument network and data archive for aerosol characterization, *Rem. Sens. Environ.*, 66, 1–16, 1998. 2.5
- Holtslag, A. A. M., and B. A. Boville, Local versus non-local boundary layer diffusion in a global climate model, *J. Clim.*, 6, 1825–1842, 1993. 2
- Husar, R. B., J. M. Prospero, and L. L. Stowe, Characterization of tropospheric aerosols over the oceans with the NOAA advanced very high resolution radiometer optical thickness operational product, *J. Geophys. Res.*, 102(D14), 16,889–16,909, 1997. 3, 3
- Iversen, J. D., and B. R. White, Saltation threshold on Earth, Mars, and Venus, *Sedimentology*, 29, 111–119, 1982. 2.1, 2.2, 2.2, 2.3
- Jenson, S. K., and J. O. Domingue, Extracting topographic structure from digital elevation data for geographic information system analysis, *Photogrammetric Engineering and Remote Sensing*, 54(11), 1593–1600, 1988. 2.6
- Kalnay, E., The NCEP/NCAR 40-year reanalysis project, *Bull. Am. Meteorol. Soc.*, 77(3), 437–471, 1996. 1, 3

- Kergoat, L., S. Moulin, P. Cayrol, and G. Dedieu, Controlling vegetation growth models with satellite measurements, in *Advances in environmental and ecological modelling*, edited by F. Blasco and A. Weill, pp. 73–89, Elsevier Publishers, 1999. 2.6
- Li, X., H. Maring, D. Savoie, K. Voss, and J. M. Prospero, Dominance of mineral dust in aerosol light-scattering in the north Atlantic trade winds, *Nature*, 380, 416–419, 1996. 2.5
- Lu, H., and Y. Shao, A new model for dust emission by saltation bombardment, *J. Geophys. Res.*, 104(D14), 16,827–16,842, 1999. 5
- Luo, C., N. M. Mahowald, C. S. Zender, and J. del Corral, A 22-year climatology of mineral aerosols, *Submitted to J. Geophys. Res.*, 2003. 1, 3, 3, 3, 3, 4
- Mahowald, N., K. Kohfeld, M. Hansson, Y. Balkanski, S. P. Harrison, I. C. Prentice, M. Schulz, and H. Rodhe, Dust sources and deposition during the last glacial maximum and current climate: A comparison of model results with paleodata from ice cores and marine sediments, *J. Geophys. Res.*, 104(D3), 15,895–15,916, 1999. 1, 2.3, 2.6, 4
- Mahowald, N. M., and J.-L. Dufresne, Sensitivity of TOMS aerosol index to boundary layer height: Implications for detection of mineral aerosol sources, *Geophys. Res. Lett.*, 31(3), L03,103, doi:10.1029/2003GL018,865, 2004. 2.6
- Mahowald, N. M., C. S. Zender, C. Luo, D. Savoie, O. Torres, and J. del Corral, Understanding the 30 year Barbados desert dust record, *J. Geophys. Res.*, 107(D21), 4561, doi:10.1029/2002JD002,097, 2002. 1
- Mahowald, N. M., C. Luo, J. del Corral, and C. S. Zender, Interannual variability in atmospheric mineral aerosols from a 22-year model simulation and observational data, *J. Geophys. Res.*, 108(D12), 4352, doi:10.1029/2002JD002,821, 2003. 1, 3
- Maring, H., D. L. Savoie, M. A. Izaguirre, C. McCormick, R. Arimoto, J. M. Prospero, , and C. Pilinis, Aerosol physical and optical properties and their relationship to aerosol composition in the free troposphere at Izaña, Tenerife, Canary Islands during July 1995, *J. Geophys. Res.*, 105(D11), 14,677–14,700, 2000. 2.5, 4
- Marticorena, B., and G. Bergametti, Modeling the atmospheric dust cycle: 1. Design of a soil-derived dust emission scheme, *J. Geophys. Res.*, 100(D8), doi:10.1029/95JD00,690, 16,415–16,430, 1995. 1, 2.1, 2.2, 2.2
- Marticorena, B., G. Bergametti, B. Aumont, Y. Callot, C. N'Doumé, and M. Legrand, Modeling the atmospheric dust cycle: 2. Simulation of Saharan dust sources, *J. Geophys. Res.*, 102(D4), doi:10.1029/96JD02,964, 4387–4404, 1997. 1, 2.3, 2.3, 5
- Martin, J. H., Glacial-interglacial CO<sub>2</sub> change: The iron hypothesis, *Paleoceanography*, 5, 1–13, 1990. 1
- Mbourou, G. N., J. J. Bertrand, and S. E. Nicholson, The diurnal and seasonal cycles of wind-borne dust over Africa north of the equator, *J. Appl. Meteorol.*, 36, 868–882, 1997. 2.6
- McKenna-Neuman, C., and W. G. Nickling, A theoretical and wind tunnel investigation of the effect of capillary water on the entrainment of sediment by wind, *Canadian Journal of Soil Science*, 69, 79–96, 1989. 2.2
- Nicholson, S. E., C. J. Tucker, and M. B. Ba, Desertification, drought, and surface vegetation: An example from the West African Sahel, *Bull. Am. Meteorol. Soc.*, 79(5), 815–829, 1998. 1, 2.6
- Owen, P. R., Saltation of uniform grains in air, *J. Fluid. Mech.*, 20(2), 225–242, 1964. 2.2
- Patterson, E. M., Optical properties of the crustal aerosol: Relation to chemical and physical characteristics, *J. Geophys. Res.*, 86(C4), 3236–3246, 1981. 2.5
- Penner, J. E., et al., Aerosols, their direct and indirect effects, in *Climate Change 2001: The Scientific Basis. Contribution of Working Group I to the Third Assessment Report of the Intergovernmental Panel on Climate Change*, edited by J. T. Houghton, Y. Ding, D. J. Griggs, M. Noguer, P. J. van der Linden, X. Dai, K. Maskell, and C. A. Johnson, chap. 5, pp. 291–336, Cambridge Univ. Press, Cambridge, UK, and New York, NY, USA, 2001. 3, 4
- Perlwitz, J., I. Tegen, and R. L. Miller, Interactive soil dust aerosol model in the GISS GCM. Part I: Sensitivity of the soil dust cycle to radiative properties of soil dust aerosols, *J. Geophys. Res.*, 106(D16), 18,167–18,192, 2001. 1, 4
- Prospero, J. M., Saharan dust transport over the North Atlantic Ocean and Mediterranean: An overview, in *The Impact of Desert Dust Across the Mediterranean*, edited by S. Guerzoni and R. Chester, pp. 133–151, Kluwer Academic Pub., Boston, MA, 1996a. 4
- Prospero, J. M., The atmospheric transport of particles to the ocean, in *Particle Flux in the Ocean, SCOPE*, vol. 57, edited by V. Ittekkot, P. Schäfer, S. Honjo, and P. J. Depetris, pp. 19–52, John Wiley & Sons Ltd., New York, 1996b. a, 3, 3, 4
- Prospero, J. M., Long-term measurements of the transport of African mineral dust to the southeastern United States: Implications for regional air quality, *J. Geophys. Res.*, 104(D13), 15,917–15,928, 1999. 1, 3
- Prospero, J. M., and R. T. Nees, Impact of the North African drought and El Niño on mineral dust in the Barbados trade winds, *Nature*, 320, 735–738, doi:10.1038/320,735a0, 1986. 4
- Prospero, J. M., P. Ginoux, O. Torres, S. E. Nicholson, and T. E. Gill, Environmental characterization of global sources of atmospheric soil dust derived from the NIMBUS7 TOMS absorbing aerosol product, *Rev. Geophys.*, 40(1), 1002, doi:10.1029/2000RG000,095, 2002. 2.6, 3, 5
- Pruppacher, H. R., and J. D. Klett, *Microphysics of Clouds and Precipitation*, 714 pp., D. Reidel Publ. Co., 1978. 2.9, 2.9
- Pye, K., *Aeolian Dust and Dust Deposits*, Academic Press, New York, NY, 1987. 2.2, 2.5
- Rasch, P. J., N. M. Mahowald, and B. E. Eaton, Representations of transport, convection, and the hydrologic cycle in chemical transport models: Implications for the modeling of short-lived and soluble species, *J. Geophys. Res.*, 102(D23), 28,127–28,138, 1997. 1, 3
- Rasch, P. J., M. C. Barth, J. T. Kiehl, S. E. Schwartz, and C. M. Benkovitz, A description of the global sulfur cycle and its controlling processes in the National Center for Atmospheric Research Community Climate Model, version 3, *J. Geophys. Res.*, 105(D1), 1367–1386, 2000. 2.9, 2.9, 2.9
- Rasch, P. J., W. D. Collins, and B. E. Eaton, Understanding the Indian Ocean Experiment INDOEX aerosol distributions with an aerosol assimilation, *J. Geophys. Res.*, 106(D7), 7337–7355, 2001. 1, 2

- Raupach, M. R., Drag and drag partition on rough surfaces, *Bound.-Lay. Meteorol.*, *60*, 375–395, 1992. 2.2
- Raupach, M. R., Simplified expressions for vegetation roughness length and zero-plane displacement as functions of canopy height and area index, *Bound.-Lay. Meteorol.*, *71*, 211–216, 1994. 2.6, 5
- Reid, J. S., et al., Comparison of size and morphological measurements of coarse mode dust particles from Africa, *J. Geophys. Res.*, *108*(D19), 8593, doi:10.1029/2002JD002,485, 2003. 2.4, 5
- Savoie, D. L., J. M. Prospero, S. J. Oltmans, W. C. Graustein, K. K. Turekian, J. T. Merrill, and H. Levy II, Sources of nitrate and ozone in the marine boundary layer of the tropical North Atlantic, *J. Geophys. Res.*, *97*(D11), 11,575–11,589, 1992. 4
- Schulz, M., Y. J. Balkanski, W. Guelle, and F. Dulac, Role of aerosol size distribution and source location in a three-dimensional simulation of a Saharan dust episode tested against satellite-derived optical thickness, *J. Geophys. Res.*, *103*(D9), 10,579–10,592, 1998. 2.1, 2.4, 2.4, 2.4
- Seinfeld, J. H., and S. N. Pandis, *Atmospheric Chemistry and Physics*, 1326 pp., John Wiley & Sons, New York, NY, 1997. 2.8.1, 2.9, a, 2.9, 2.9
- Selah, A., and D. W. Fryrear, Threshold wind velocities of wet soils as affected by wind blown sand, *Soil Science*, *160*(4), 304–309, 1995. 2.2
- Shao, Y., A model for mineral dust emission, *J. Geophys. Res.*, *106*(D17), 20,239–20,254, 2001. 1
- Shao, Y., and L. M. Leslie, Wind erosion prediction over the Australian continent, *J. Geophys. Res.*, *102*(D25), 30,091–30,105, 1997. 1, 2.3
- Shao, Y., M. R. Raupach, and P. A. Findlater, Effect of saltation bombardment on the entrainment of dust by wind, *J. Geophys. Res.*, *98*(D7), 12,719–12,726, 1993. 2.3
- Shao, Y., M. R. Raupach, and J. F. Leys, A model for predicting aeolian sand drift and dust entrainment on scales from paddock to region, *Aust. J. Soil Res.*, *34*(D25), 309–342, 1996. 1, 2.1, 2.2, 2.2, 2.3
- Shettle, E. P., Optical and radiative properties of a desert aerosol model, in *IRS '84: Current Problems in Atmospheric Radiation*, edited by G. Fiocco, August 21–28, Perugia, Italy, pp. 74–77, Proceedings of the International Radiation Symposium, A. Deepak, Hampton VA, 1984. 2.4
- Shinn, E. A., G. W. Smith, J. M. Prospero, P. Betzer, M. L. Hayes, V. Garrison, , and R. T. Barber, African dust and the demise of Caribbean coral reefs, *Geophys. Res. Lett.*, *27*(19), 3029–3032, 2000. 1
- Slinn, W. G. N., L. Hasse, B. B. Hicks, A. W. Hogan, D. Lal, P. S. Liss, K. O. Munnich, G. A. Sehmel, and O. Vittori, Some aspects of the transfer of atmospheric trace constituents past the air-sea interface, *Atmos. Environ.*, *12*, 2055–2087, 1978. 2.8.2
- Sokolik, I. N., and O. B. Toon, Direct radiative forcing by anthropogenic airborne mineral aerosols, *Nature*, *381*, 681–683, 1996. 2.5
- Sokolik, I. N., A. V. Andronova, and T. C. Johnson, Complex refractive index of atmospheric dust aerosols, *Atmos. Environ.*, *27A*, 2495–2502, 1993. 2.5
- Sokolik, I. N., D. M. Winker, G. Bergametti, D. A. Gillette, G. Carmichael, Y. J. Kaufman, L. Gomes, L. Schuetz, and J. E. Penner, Introduction to special section: Outstanding problems in quantifying the radiative impacts of mineral dust, *J. Geophys. Res.*, *106*(D16), 18,015–18,027, 2001. 2.5
- Stowe, L. L., A. M. Ignatov, and R. R. Singh, Development, validation, and potential enhancements to the second-generation operational aerosol product at the National Environmental Satellite, Data, and Information Service of the National Oceanic and Atmospheric Administration, *J. Geophys. Res.*, *102*(D14), 16,923–16,934, 1997. 3
- Swap, R., M. Garstang, S. Greco, R. Talbot, and P. Källberg, Saharan dust in the Amazon Basin, *Tellus*, *44B*, 133–149, 1992. 1, 3
- Tegen, I., and I. Fung, Modeling of mineral dust in the atmosphere: Sources, transport, and optical thickness, *J. Geophys. Res.*, *99*(D11), 22,897–22,914, 1994. 1, 2.3, 3, b, 3, 4
- Tegen, I., and I. Fung, Contribution to the atmospheric mineral aerosol load from land surface modification, *J. Geophys. Res.*, *100*(D9), 18,707–18,726, 1995. 2.6, 3
- Tegen, I., A. A. Lacis, and I. Fung, The influence on climate forcing of mineral aerosols from disturbed soils, *Nature*, *380*, 419–422, 1996. 1, 4
- Torres, O., P. K. Bhartia, J. R. Herman, Z. Ahmad, and J. Gleason, Derivation of aerosol properties from satellite measurements of backscattered ultraviolet radiation: Theoretical basis, *J. Geophys. Res.*, *103*(D14), 17,099–17,110, 1998. 2.6
- Webb, R. S., C. E. Rosenzweig, and E. R. Levine, Specifying land surface characteristics in general circulation models: soil profile data set and derived water-holding capacities, *Global Biogeochem. Cyc.*, *7*, 97–108, 1993. 2.3
- Wesely, M. L., Parameterization of surface resistances to gaseous dry deposition in region-scale numerical models, *Atmos. Environ.*, *23*(6), 1293–1304, 1989. 2.8.2
- White, B. R., Soil transport by winds on Mars, *J. Geophys. Res.*, *84*(B9), 4643–4651, 1979. 2.3, 2.3
- Wiscombe, W. J., and S. G. Warren, A model for the spectral albedo of snow. I: Pure snow, *J. Atmos. Sci.*, *37*, 2712–2733, 1980. 2.6
- Woodward, S., Modeling the atmospheric lifecycle and radiative impact of mineral dust in the Hadley Centre climate model, *J. Geophys. Res.*, *106*(D16), 18,155–18,166, 2001. 1, 2.3, 3, 4, 4
- Zender, C. S., D. J. Newman, and O. Torres, Spatial heterogeneity in aeolian erodibility: Uniform, topographic, geomorphic, and hydrologic hypotheses, *J. Geophys. Res.*, *108*(D17), 4543, doi:10.1029/2002JD003,039, 2003. 2.6
- Zhang, G. J., and N. A. McFarlane, Sensitivity of climate simulations to the parameterization of cumulus convection in the Canadian Climate Centre general circulation model, *Atmos. Ocean*, *33*(3), 407–446, 1995. 2
- Zhang, Y., C. Seigneur, J. H. Seinfeld, M. Jacobson, S. L. Clegg, and F. S. Binkowski, A comparative review of inorganic aerosol thermodynamic equilibrium modules: Similarities, differences, and their likely causes, *Atmos. Environ.*, *34*, 117–137, 2000. 2.9
- H. Bian, D. Newman, C. S. Zender, Department of Earth System Science, University of California, Irvine, CA 92697-3100. (zender@uci.edu)

This preprint was prepared with AGU's L<sup>A</sup>T<sub>E</sub>X macros v5.01, with the extension package 'AGU++' by P. W. Daly, version 1.6b from 1999/08/19.